Carbon-Based Materials for Oxidative Desulfurization and Denitrogenation of Fuels: A Review

Fernanda F. Roman [1,2,3], Jose L. Diaz de Tuesta [1], Adrián M. T. Silva [2,3], Joaquim L. Faria [2,3] and Helder T. Gomes [1,*]

[1] Centro de Investigação de Montanha (CIMO), Instituto Politécnico de Bragança, 5300-253 Bragança, Portugal; roman@ipb.pt (F.F.R.); jl.diazdetuesta@ipb.pt (J.L.D.d.T.)
[2] Laboratory of Separation and Reaction Engineering—Laboratory of Catalysis and Materials (LSRE-LCM), Faculdade de Engenharia, Universidade do Porto, 4200-465 Porto, Portugal; adrian@fe.up.pt (A.M.T.S.); jlfaria@fe.up.pt (J.L.F.)
[3] ALiCE—Associate Laboratory in Chemical Engineering, Faculdade de Engenharia, Universidade do Porto, 4200-465 Porto, Portugal
[*] Correspondence: htgomes@ipb.pt

Abstract: Sulfur (S) and nitrogen (N) are elements naturally found in petroleum-based fuels. S- and N-based compounds in liquid fuels are associated with a series of health and environmental issues. Thus, legislation has become stricter worldwide regarding their content and related emissions. Traditional treatment systems (namely hydrodesulfurization and hydrodenitrogenation) fail to achieve the desired levels of S and N contents in fuels without compromising combustion parameters. Thus, oxidative treatments (oxidative desulfurization–ODS, and oxidative denitrogenation-ODN) are emerging as alternatives to producing ultra-low-sulfur and nitrogen fuels. This paper presents a thorough review of ODS and ODN processes applying carbon-based materials, either in hybrid forms or as catalysts on their own. Focus is brought to the role of the carbonaceous structure in oxidative treatments. Furthermore, a special section related to the use of amphiphilic carbon-based catalysts, which have some advantages related to a closer interaction with the oily and aqueous phases, is discussed.

Keywords: desulfurization; denitrogenation; carbon catalysts; carbon composites; biphasic oxidation; amphiphilic material; low-sulfur fuels; liquid fuels

1. Introduction

With increasing urbanization, humankind has experienced an escalating dependence on energy. As shown in Figure 1, for EU-28, total energy supply amounted to 1.58M toe (tonnes of oil equivalent) in 2019, and oil and petroleum products represented the highest contribution (32.8%), followed by natural gas (25%), renewables and biofuels (15.8%), nuclear heat (13.2%), and solid fossil fuels (11%). In particular, the contribution of oil and petroleum products in energy supplies has kept with no relevant changes (31.4–33.0%) in the last decade (Figure 1a), with values ranging from 510k (2014) to 569k (2010) toe. Oil and petroleum products are extensively used in our society for transportation, electricity, and construction materials. Transportation may be the sector that most relies on petroleum-based fuels, from ground transportation to planes and ships. In EU-28, the final consumption of energy in the transport sector amounted to 330.8k toe in 2019, being 209.8k toe of gas oil and diesel, 79.1k toe of motor gasoline, 17.4k toe of renewables and biodiesel, and 3.7k toe of natural gas (Figure 1b). In the last decade, gasoline consumption has decreased from 28.5% to 23.9% of the total energy consumed in the transportation sector, whereas gas oil and diesel have increased from 60.7% to 63.4% (Figure 1b).
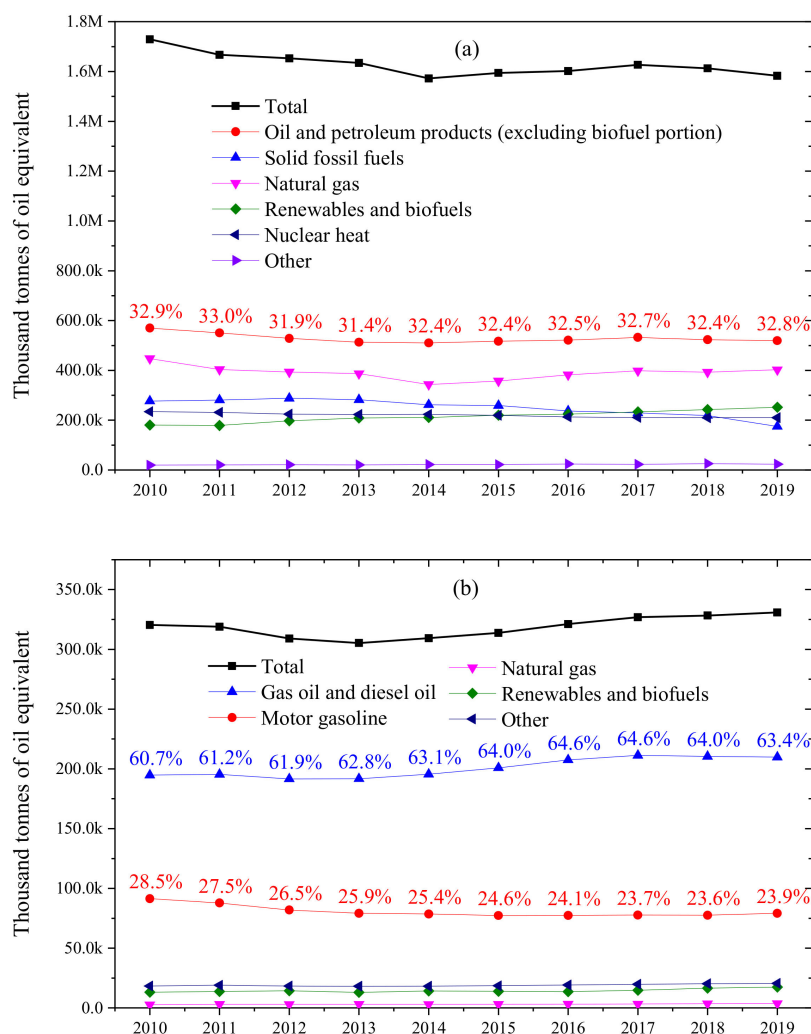
Figure 1. Evolution of (**a**) total energy supply and (**b**) final consumption in the transport sector (only energy use) in EU 28. Source: Eurostat [1].

Some heteroatoms are inherently found in petroleum and petroleum-based fuels. The atom found in the highest concentration after carbon and hydrogen is sulfur, followed by nitrogen. Their presence is associated with a series of environmental and health-related issues due to the formation of toxic gaseous products (NO_x and SO_2) during combustion. Those issues have driven legislative bodies to regulate the content and related emissions of S- and N-based compounds, increasing restrictions. Hydrodesulfurization (HDS) and hydrodenitrogenation (HDN) are the technologies applied at the industrial level. However, HDS and HDN fail to achieve the required-by-law content of sulfur without compromising relevant combustion parameters of the fuels (such as diesel and gasoline). Alternative technologies have been studied in the last few years and, among them, oxidative treatments can be highlighted, namely oxidative desulfurization (ODS) and denitrogenation (ODN). As with any catalytic process, the development and selection of catalysts are critical in ODS and ODN, and carbon-based materials have revealed exciting results in the oxidative removal of S- and N-based compounds. This review aims to discuss the state-of-the-art application of carbon-based materials for ODS and ODN purposes, emphasizing the role displayed by those materials, either in hybrid forms or as carbocatalysts.

1.1. Sulfur and Nitrogen in Crude Oils: Content and Type of Compounds

Petroleum is composed mostly of hydrocarbons, although impurities such as nitrogen, sulfur, oxygen, and metal compounds (vanadium, nickel, and iron, among others) are found [2]. Sulfur is the component that varies the most between different petroleum samples [2] and is the third most abundant element in crude oils, after carbon and hydrogen [3]. Sulfur content can vary between <0.1 to 8 wt.% [2], leading to the classifications of sweet crude oils (S content <1 wt.%) or sour oils (S content >1 wt.%) [3]. Nitrogen content can vary between <0.1 to 1.8 wt.% [2], and crudes can be classified as high-nitrogen oils (>0.25 wt.%) or nitrogen-poor oils (<0.25 wt.%) [4]. Table 1 displays some examples of the content of sulfur and nitrogen in different crude oil samples. There is no correlation between the content of sulfur and nitrogen. The content of those impurities depends mostly on the area of exploration [4,5].

Table 1. Sulfur and nitrogen content for crude oil in different regions.

Local of Exploration	Type of Oil	S Content (wt.%)	N Content (wt.%)
USA, AR, Atlanta	Petroleum (Light oil)	0.37	0.003
USA, CA, Temblor	Petroleum (Medium oil)	0.44	0.27
USA, CA, Oxnard	Petroleum (Heavy oil)	7.47	0.88
USA, MS, Eucutta	Petroleum (Heavy oil)	3.89	0.13
Iran, Agha-Jeri	Petroleum (Light oil)	1.36	0.14
Greece, Keri	Petroleum (Heavy oil)	5.76	0.17
Australia, Pumpherston	Shale oil (Medium oil)	0.56	0.52
France, Petit	Shale oil (Medium oil)	3.40	0.65
South Africa, Salermo	Shale oil (Medium oil)	0.64	0.85
Sweden, Lundstrom	Shale oil (Light oil)	0.71	0.11

Source: adapted from Ball, Whisman, and Wenger (1951) [6].

S-containing compounds found in petroleum can be divided into four main groups: mercaptans (R-SH), sulfides (R_2S), disulfides (RSSR), and thiophenes. Some examples of these compounds can be seen in Figure 2. Other compounds may include H_2S and elemental sulfur, although in trace quantities [7]. N-containing compounds are classified into two major groups: basic (derived from pyridine) and non-basic or neutral (derived from pyrrole) [4]. Figure 3 displays some N-containing compounds commonly found in petroleum. There is also evidence of the presence of primary amines (R-NH_2), porphyrins structures, or compounds that contain nitrogen and oxygen simultaneously [4].
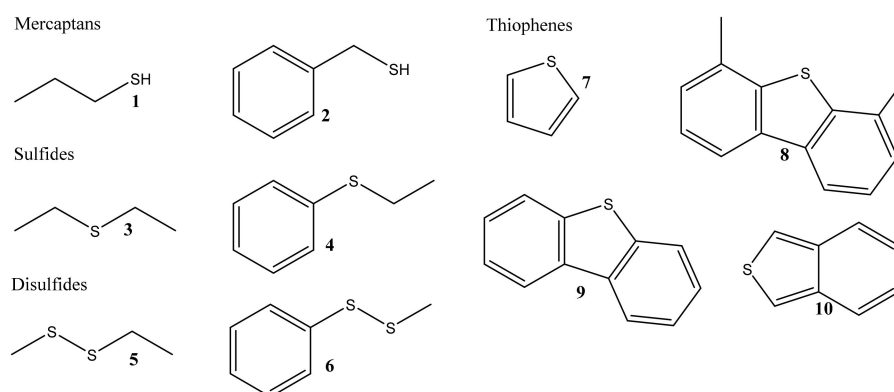
Figure 2. Examples of S-containing compounds found in petroleum. Mercaptans: propane-1-thiol **1**, phenylmethanethiol **2**. Sulfides: diethylsulfane **3**, ethyl phenyl sulfide **4**. Disulfides: (methyldisulfanyl)methane **5**, methyl phenyl disulfide **6**. Thiophenes: thiophene (Th) **7**, 4,6-dimethyldibenzothiophene (4,6-DMDBT) **8**, dibenzothiophene (DBT) **9**, and benzothiophene (BT) **10**.
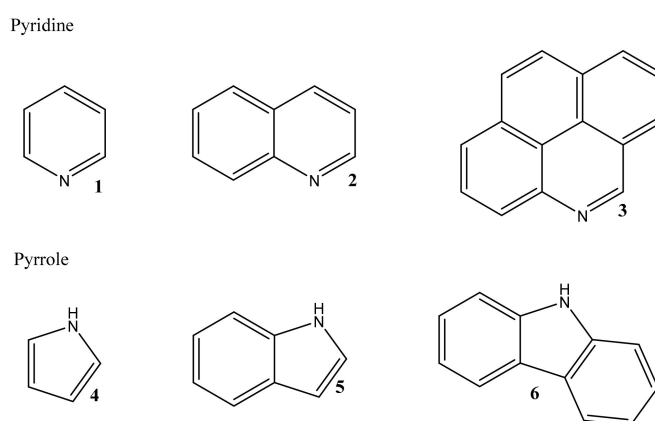
Pyridine

Pyrrole

Figure 3. Examples of N-containing compounds found in petroleum. Pyridines group: pyridine **1**, quinoline (QN) **2**, azapyrene **3**. Pyrroles group: pyrrole **4**, indole **5**, and carbazole **6**.

Heavier boiling fractions contain higher amounts of sulfur compounds (main boiling fractions are displayed in Figure 4). In the gasoline boiling range, mercaptan, sulfide, disulfide, and thiophene groups are found. In contrast, jet fuel and diesel primarily include thiophenes and derivatives [8]. Similarly, the nitrogen content increases for heavier fractions. Most N-compounds occur in the residual boiling fractions [4].
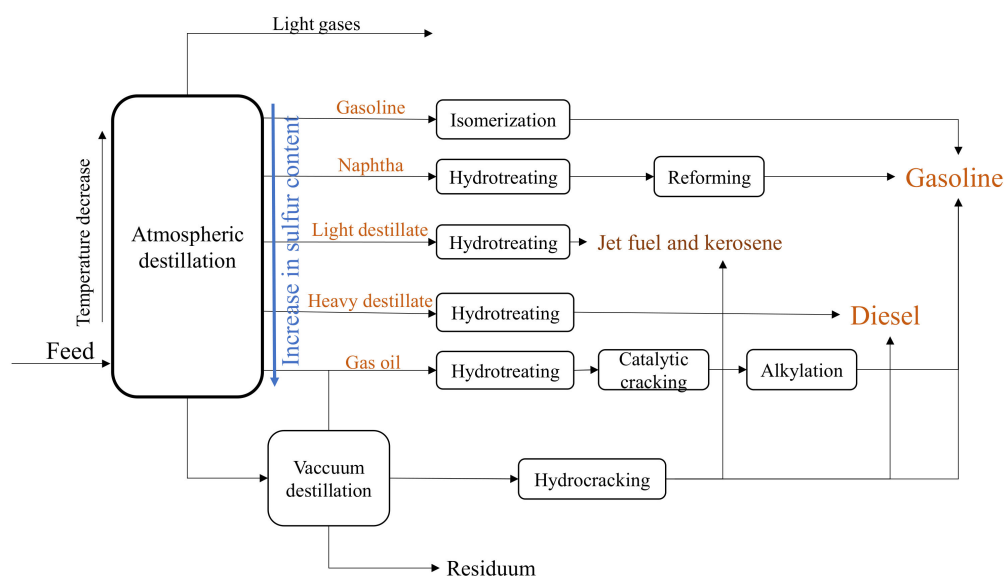
Figure 4. Simplified flowchart of a petroleum refinery and its main boiling fractions. Adapted from Romanow-Garcia and Hoffman (2003) [9].

1.2. Health, Environmental and Technological Effects of Sulfur- and Nitrogen-Containing Compounds

Upon combustion of petroleum-based fuels, hazardous gases (SO_2 and NO_x) and particulate matter (PM) are released [10]. PM can be generated directly during combustion (primary PM) or from the chemical reaction of exhaust gases, including SO_2 and NO_x (secondary PM). The exact composition of the exhaust gas depends on a series of factors, mainly fuel composition and combustion conditions. However, PM and NO_x emissions can be controlled by augmenting the cetane number and lowering the number of aromatic compounds in diesel fuels [10], besides reducing the content of N-containing compounds. Reducing the content of sulfur diminishes SO_2 and sulfur-based PM [10].

Exposure to SO_2 and NO_x is related to several health issues in humans. NO_x and SO_2 are both irritants of the respiratory system and are associated with worsening existing respiratory illnesses, such as asthma, and increased susceptibility to lung infections [11]. Most of the PM emitted in diesel engines (>90%) is smaller than 1 μm in diameter [10]. PM_{10} (aerodynamic diameter <10 μm) is a nose and throat irritant, causing lung damage, bronchitis, and risk of cardiac arrest, which is even associated with early death [12]. Studies have shown that long-term exposure to diesel combustion products is associated with a 20–50% increase in the likelihood of developing lung cancer due to genotoxicity [10,13]. Similarly, exposition to diesel exhausts is related to a 4-fold increase in the risk of dying of noncancerous diseases, such as cardiovascular diseases [10]. A study done in 2003 found a positive correlation between exposure to an increased daily concentration of SO_2 in the atmosphere and hospital admissions for cardiovascular diseases and ischemic heart diseases in major European cities [14]. Mortality and morbidity rates due to SO_2 exposure result in relevant monetary costs, as estimated by Wu et al. (2020) (35.76 and 441.47 million RMB Yuan, respectively, for Beijing, China, in 2016) [15].

NO_x and SO_2 also provoke adverse environmental effects. NO_x and SO_2 from exhaust engines combine with air moisture and contribute to acid rain [10]. Acid rain is linked to the depletion of essential soil nutrients, affecting soil fertility [7]. Soil pH is also altered, destroying some microbial cultures [7]. Soil alterations threaten forest vegetation and crop production. It contributes to dissolving harmful substances (such as heavy metals), leaching to water bodies. It is also associated with lake acidification and water nitrification [16,17], impacting microorganisms' reproduction and growth. Acid rain also affects human-made structures, diminishing the lifespan of buildings, bridges, statues, among others [7,17]. Furthermore, both primary and secondary PM reduce atmospheric visibility between 8 and 25% [10].

Sulfur compounds, mainly H_2S and mercaptans, are related to a strong odor in sour petroleum [7]. Furthermore, lower aliphatic sulfides and mercaptans are highly reactive towards metals and cause corrosion, damaging storage tanks, pipelines, and equipment [7]. However, the main issue with S-containing compounds during refining is the deactivation of metal catalysts in downstream units [7]. In hydrogenation, reforming, isomerization, and alkylation processes, sulfur is adsorbed in the catalyst surface. Sulfur adsorption then hinders the adsorption of any other species. The deactivation degree depends on the extension of the active sites that were obstructed. Depending on the metal used as catalyst, irreversible poisoning can happen, and thus the regeneration of the catalyst becomes a difficult task [7]. Additionally, sulfur chemisorbs on the catalysts used in the catalytic converter (responsible for reducing CO and NO_x emissions in passengers' vehicles), causing catalyst deactivation and reducing engine efficiency [5,18].

N-containing compounds pose issues in catalyst selection and process development and operation in oil upgrading and refining [4]. The main problems associated with nitrogen are: (i) 5-membered rings containing nitrogen compounds, such as pyrrolic compounds, are prone to free radical addition reactions, forming heavier products or gums that highly compromise storage stability [4]; (ii) the presence of basic nitrogen compounds leads to the deactivation of acid catalysts through acid–base reactions [4]; (iii) the presence of basic nitrogen compounds leads to salt precipitation (due to acid–base reactions with carboxylic acids), resulting in equipment fouling and even corrosion if water is present under high-temperature operation [4]; (iv) metal coordination is indirectly controlled by nitrogen, and nitrogen is therefore indirectly responsible for metal deposition, leading to equipment fouling [4]; (v) nitrogen competes with other compounds for active sites on catalyzed processes, such as the HDS process. Thus, the presence of nitrogen compounds hinders the removal of sulfur compounds [4]. Therefore, it is preferable to remove nitrogen compounds, especially before the refining processes.

1.3. Legislation

The maximum sulfur content allowed for transportation fuels (gasoline and diesel) has become stricter in the last years worldwide. Currently, the EU allows only 10 ppm of sulfur in diesel and gasoline [19]. In contrast, the US limits of sulfur content for gasoline and diesel are 10 [20] and 15 ppm [21], respectively. Figure 5 shows the evolution of the allowed content of sulfur in gasoline (Figure 5a) and diesel (Figure 5b) in the last decades. As observed, EU was first to regulate the content of sulfur in gasoline to 150 ppm in 2000, followed by Australia (500 ppm in 2002) > Canada (150 ppm in 2003) > US (120 ppm in 2004) > India (500 ppm in 2005) > China (500 ppm in 2006) > Japan (10 ppm in 2007) > Brazil (50 ppm in 2010) > Russia (150 ppm in 2013). However, the most restricted content of sulfur in gasoline (10 ppm) was first established by Japan in 2007, followed by Canada and EU (2009) > Russia (2016) > US and China (2017) > India (2020) and Australia (2027, to be implemented). For diesel (Figure 5b), Japan was also the first to limit the S-content in 10 ppm in 2007, followed by EU and Australia (2009), Brazil (2013), Russia (2016), China (2017), and India (2020) (the US and Canada establish the value of 15 ppm). Nitrogen is not directly regulated in permitted content but indirectly by allowed NO_x emissions, gum content, storage, and thermal stability [4].
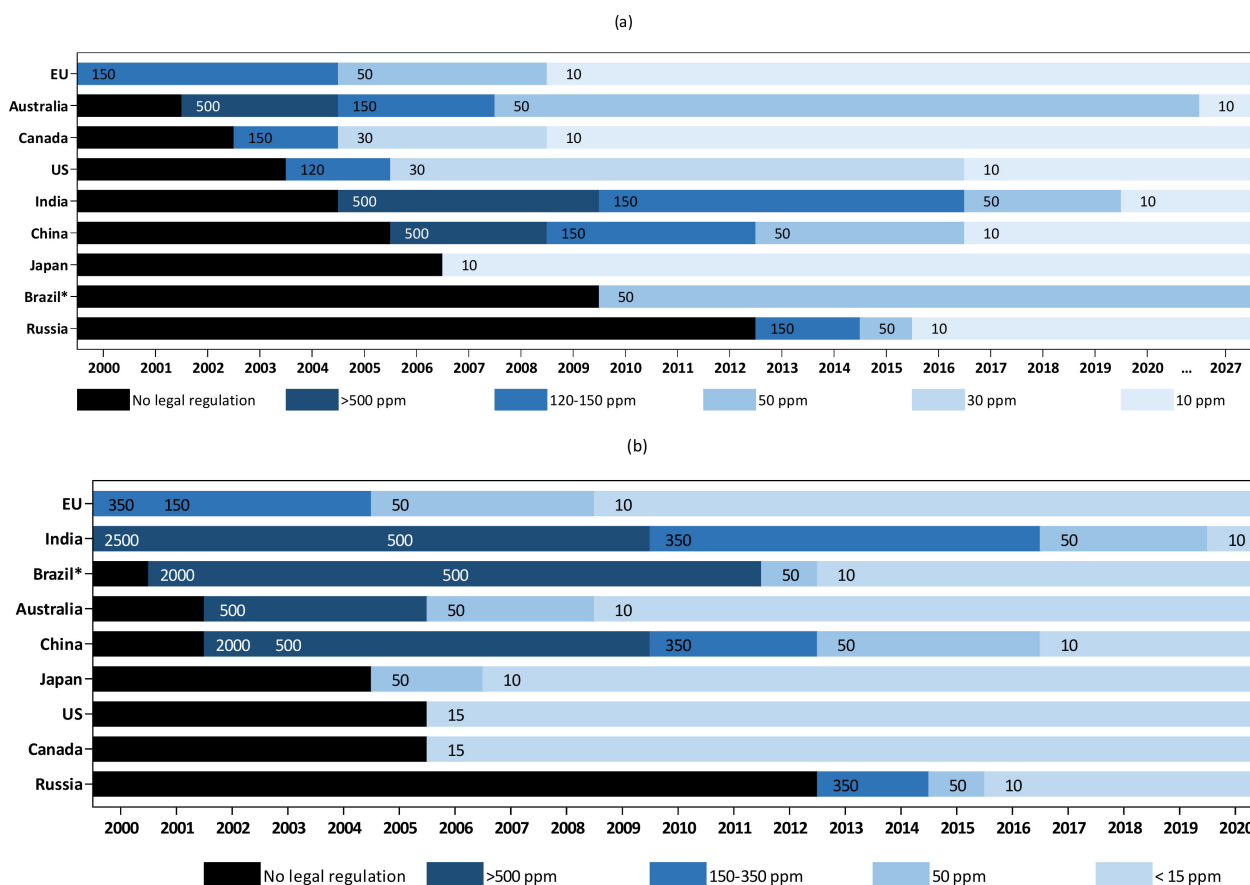
Figure 5. Evolution of the limit of sulfur content in (**a**) gasoline and (**b**) diesel, according to the implementation date. * Refers to metropolitan areas. Source: Miller and Façanha (2014) [22], TransportPolicy.net [23–26], United States Environmental Protection Agency [20], Australian Government [27], Euro V [28], Miller, and Jin (2019) [29].

2. Processes for Removal of Sulfur and Nitrogen from Fuels

Environmental issues and restrictive legislation have spiked the interest desulfurization and denitrogenation technologies since 1951 (Figure 6). The most studied strategies are classified in conventional processes, as HDS and HDN, and in more novel approaches, mainly ODS and ODN.
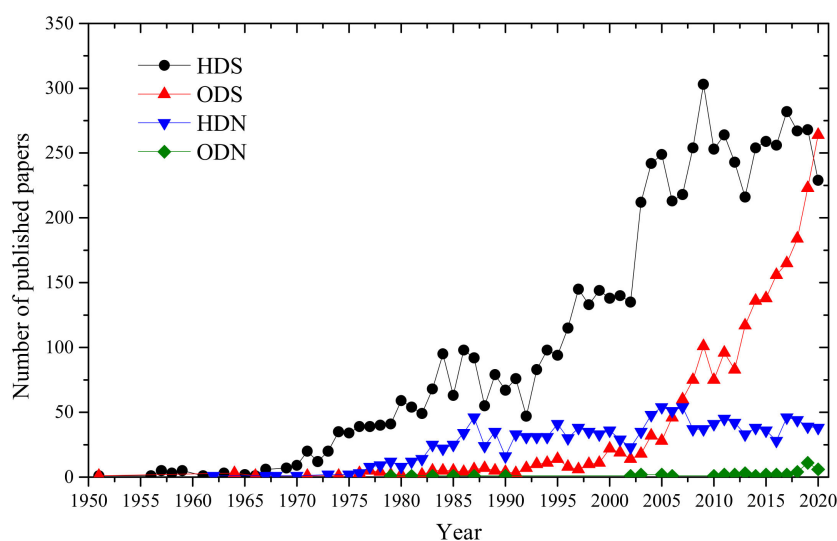
Figure 6. Papers published on HDS, HDN, ODS, and ODN over the years (source: SCOPUS with the keywords "hydrodesulfurization," "hydrodenitrogenation," "oxidative desulfurization," and "oxidative denitrogenation," respectively, dated August 2021).

2.1. Hydrodesulfurization (HDS) and Hydrodenitrogenation (HDN)

Several processes based on the reaction between hydrocarbons and hydrogen are used in the petroleum industry, such as hydrotreating, hydrocracking, and hydrogenation [30]. Hydrotreating refers to removing undesired species, such as sulfur, nitrogen, oxygen, and metal impurities, from petroleum fractions [30] by hydrogenolysis of C-X bonds, where X can be S, N, O, or metal. The net result is the formation of C-H bonds (hydrogenation) and H-X bonds [30]. The chemical reaction of fixating a hydrogen atom onto a hydrocarbon double bond, known as hydrogenation, using nickel catalysts, was first described in 1897. However, only in the mid-50s, the first noble metal catalyst was developed, and the HDS process commercialized [31]. Several HDS processes have been commercialized from then on, and all petroleum refineries worldwide have at least one hydrotreating unit [31].

The hydrotreatment of nitrogen-, sulfur- and oxygen-containing compounds will lead to ammonia (NH_3), hydrogen sulfide (H_2S), and water, respectively [31]. Oxygen-containing compounds are much more reactive than nitrogen- and sulfur-containing compounds towards hydrotreatment, and thus hydrotreating is not specifically developed to remove O-compounds [32]. Most processes are designed to deal with S-compounds due to their hazardous effect on downstream processes. The removal of S, N, and other impurities co-occur in refinery conditions [33]. Thus, N-containing impurities are also removed during hydrotreatment processes designed to remove sulfur [32], although nitrogen compounds are much less reactive and hard to remove than sulfur [4].

Different sulfur compounds have different rates of HDS [32]. Mercaptans, sulfides, and disulfides are highly reactive towards HDS under mild conditions. On the other hand, 5-membered ring compounds containing sulfur (thiophenes) are very little reactive towards HDS, and the reactivity decreases as the number of rings (in the range 1–3 rings) increases [32]. However, the tendency reverses for structures containing four or more rings, and the reactivity increases as the number of rings increases [32]. The distinct behavior is that there is more than one pathway to remove sulfur from a molecule. Depending on the sulfur compound, one pathway may be more relevant than the other [32]. The order of reactivity of common organosulfur compounds towards HDS can be seen in Figure 7.

harder   order of reactivity towards HDS   easier
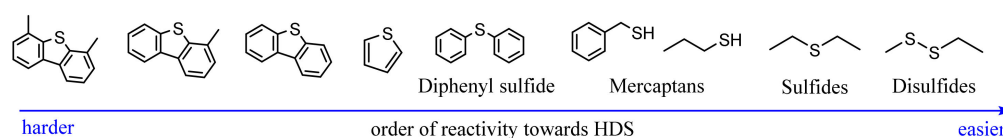
Figure 7. Order of reactivity of different S-containing compounds. Adapted from Rajendran et al. (2020) [34].

Analogous to thiophenes, nitrogen-containing compounds require a step of hydrogenation before removal of N, and thus, the H_2 partial pressure is crucial [33]. Nitrogen removal for pyridinic structures is more complex than for thiophene structures. One single bond and one double bond require to be broken [4]. In contrast, thiophenes only require two single bonds to be broken [4]. The presence of alkyl groups tends to decrease the reactivity of the S-compounds due to steric hindrance. The closer the alkyl group is to the sulfur or nitrogen atom, the stronger the effect on the reactivity [33]. Further information regarding the effect of temperature, catalysts, and other parameters in HDS and HDN processes may be found elsewhere [35].

Thus, different operating conditions may be required depending on the compounds present in the petroleum fraction. Table 2 shows some common hydrotreatment operational conditions for different fractions of petroleum. Heavier fractions tend to be richer in thiophene and N-containing compounds, and harsher conditions are required to remove those compounds. Increasing operational conditions affects a series of parameters in diesel and gasoline. Oxygen, benzene, aromatics and olefin contents, vapor pressure, and boiling range can be compromised during gasoline range hydrotreatment. In contrast, the compromised parameters for diesel are cetane number, density, and content on polynuclear aromatics and distillation 95% point for diesel [36]. Besides that, hydrogen is a very expensive reactant, and process efficiency is highly limited by the reactivity of certain sulfur compounds, by the deactivation of catalysts due to coke formation, and by the presence of H_2S [7]. Thus, alternatives to HDS and HDN processes need to be sought.

Table 2. Process conditions for different fractions of petroleum for HDS.

Feed	Temperature (°C)	Hydrogen Partial Pressure (bar)	Hydrogen Consumption (wt.%)	Catalyst Life Span (Years)
Naphta	260–300	5–10	0.05–0.10	3–10
Kerosene	300–340	15–30	0.10–0.20	–
Gas oil	320–350	15–40	0.30–0.50	–
Residue	340–425	55–170	1.50–2.00	0.5–1

Source: adapted from Fahim et al. (2010) [30] and Speight (2011) [31].

2.2. Alternative Routes to Remove Sulfur and Nitrogen

There is a wide range of alternatives to remove sulfur and nitrogen from liquid fuels. There are approaches based on liquid–liquid extraction (extractive desulfurization–EDS) using traditional solvents, deep eutectic solvents (DES) or ionic liquids (ILs) [37–39], adsorption (adsorptive desulfurization–ADS) [40], microorganisms (biodesulfurization–BDS) [41], and the oxidation of the undesired compounds (e.g., oxidative desulfurization-ODS). ODS is a promising technology since it operates under milder temperature and pressure conditions (25–140 °C, 1–2 bar) than HDS (260–425 °C, 5–160 bar). Thus, ODS does not require specialized reactors to operate at high pressure and temperature conditions. Catalyst and solvents can be mostly recycled, and the refractory-towards-HDS sulfur compounds are easily oxidized, leading to deep desulfurization [7]. Finally, ODS does not cause olefins saturation, nor does it result in loss of octane content [42] or other fuel parameters as those affected during HDS under harsher conditions.

Oxidative Desulfurization (ODS) and Denitrogenation (ODN)

The ODS process is based on the oxidation of sulfur-containing compounds towards their corresponding sulfoxides and sulfones (as shown in Figure 8) [43], followed by the extraction or adsorption of the oxidized compound. Thus, ODS is, in fact, a two-step process: (i) oxidation and (ii) extraction (or adsorption) [7,43] of the oxidized compounds. In some cases, especially with ILs, which can act as catalysts and extractants in ODS, an alternative system, extractive-catalytic oxidative desulfurization (ECODS), is introduced [44].
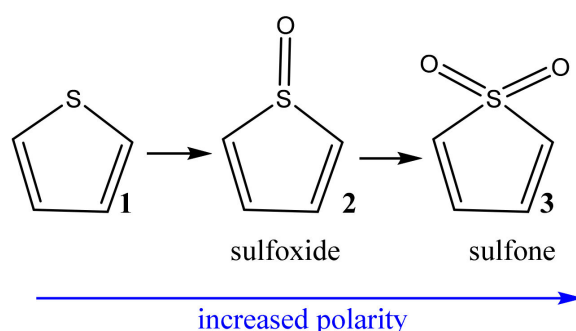
Figure 8. Oxidation of thiophene (Th) **1** to a sulfoxide (thiophene 1-oxide **2**) and a sulfone (thiophene 1,1-dioxide **3**).

Due to the strong affinity of sulfur for oxygen, oxidation of hydrocarbons is not expected to occur in the usual operating conditions of ODS, thus promoting the selective oxidation of organosulfur compounds without affecting C-C bonds [34]. The reactivity of a sulfur compound towards oxidation depends on the electron density around the S atom. The higher the electron density, the more prone the electrophilic attack on the oxygen is [7] and the higher is the reaction rate towards the formation of sulfones [45]. However, the order of reactivity seems to depend significantly on the type of oxidant, catalyst, and operating conditions. Nevertheless, there is no organosulfur category that is entirely unreactive towards ODS [34].

The ODN process, in turn, has not been as extensively studied as ODS (as demonstrated in Figure 6). There is a broader range of possible reaction products than ODS during the oxidation of N-containing compounds due to the several bonds of N-compounds that are prone to oxidation [46]. For instance, quinoline (QN) oxidation gives reaction intermediates: 5-hydroxyquinoline and 8-hydroxyquinoline are the major products. However, trace quantities of 3-, 6- and 7-hydroxyquinoline are also observed [47]. Selectivity towards one product or the other may be tuned by controlling the reaction conditions [46].

Several oxidants have been reported in the literature for ODS and ODN, such as hydrogen peroxide, organic peracids, oxygen, and ozone, among others [7]. The oxidized compounds have an increased relative polarity compared to their parent compounds, and thus their extraction is facilitated [5]. The oxidized compounds are more commonly removed through liquid–liquid extraction rather than through adsorption. Adequate extractants should fulfill a few criteria: they should be immiscible with the oil phase, they should be able to dissolve sulfones and sulfoxides, differences in density may exist to facilitate the separation between oil and extractant, and not impact the fuel properties, among others [34]. Some extractants found in the literature are acetonitrile (ACN), methanol (MeOH), ethanol (EtOH), diethyl ether (Et$_2$O), dimethylformamide (DMF), methyl cyanide, carbon tetrachloride (CCl$_4$), and ILs. Aqueous solutions of H$_2$O$_2$ (used as an oxidant) also are applied as extractants on their own.

As previously mentioned, both ODS and ODN are primarily conducted in a two-step process. However, in order to cut costs and accelerate the processes, one-pot approaches are increasingly sought. In one-pot approaches, extraction occurs concomitantly to oxidation and, hence, the extractant must be present during the oxidation step. Proper extractants are immiscible with the oil phase and, thus, one-pot approaches are commonly conducted in a biphasic medium. Biphasic systems have some advantages over traditional homogeneous systems. Biphasic systems allow conducting reactions with reactants with distinct solubility behaviors. They allow an easier separation between reactants, products, and catalysts, and the reactions to be conducted with incompatible substances, avoiding interferences [48,49].

However, biphasic systems display some issues. The main issue is the low interfacial area between the phases, hindering reaction [48,50]. An alternative is emulsifying the biphasic medium [48], as emulsion systems significantly improve the interfacial area. Emulsifying requires the use of a surfactant or of solid particles that allow the stabilization of Pickering emulsions. Pickering emulsions are an exciting template since the solid particles act as stabilizers and can also assume the role of catalysts. This approach is often referred to as Pickering Interfacial Catalysis (PIC) [50,51].

A wide range of solid particles can be used in the stabilization of Pickering emulsions, such as silica [52], magnetic particles [53], and carbon-based materials [54,55], among others. Pickering emulsions are affected by a range of conditions (pH, type of oil, ratio between the 2 phases, and concentration of particles, among others). One of the most interesting strategies to adjust emulsion formation and stability is to tune the amphiphilic character of the solid particles [56]. Amphiphilic materials display both hydrophilic and hydrophobic character and thus are wetted by more than one phase. As expected, particles wetted by more than one phase should allow easier emulsion formation and more stable emulsions [56]. Thus, amphiphilic materials should be advantageous when working under biphasic systems, especially in PIC-like approaches under emulsified systems.

Numerous catalysts have been applied for ODS and ODN purposes. However, discussing possible catalysts rather than carbon materials is not the aim of this review. Further information on other ODS catalysts may be found elsewhere [34,42,44,57]. Carbon-based materials, i.e., the focus of this review, have been widely used in ODS and ODN, either by composing hybrid materials or as catalysts on their own. Carbon-based materials display several advantages in oxidative processes. Their ability to form oxidizing species (such as hydroxyl radicals) from oxidant sources (such as hydrogen peroxide) has been widely studied [58–62]. They are proven catalysts for oxidation reactions in the liquid phase, either as catalysts on their own or in hybrid forms, such as in water and wastewater remediation [63–67]. Thus, applying those materials in the oxidative removal of sulfur and nitrogen from liquid fuels is a natural extension. Carbon-based materials can be synthesized from various precursors, including waste materials [68–70], and through several synthesis procedures [68–75]. Table 3 summarizes the main carbon-based materials that will be discussed in the following sections, along with some common carbon sources and synthesis routes. The column with the reference will lead the reader to the appropriate literature regarding the preparation of the mentioned materials.

In the following section, papers related to ODS and ODN of liquid fuels (simulated or real matrix) using strictly carbon-based materials in hybrid forms or as catalysts on their own will be presented. Furthermore, when appropriate, a distinction between the papers that use a two-step process, a biphasic system, and a PIC-type approach will also be made.

Table 3. Examples of carbon-based materials, and respective carbon precursors, synthesis routes and characteristics, studied for ODS and ODN purposes.

Carbon-Based Material	Carbon Source	Synthesis Procedures	Characteristics	Ref.
Carbon Nanotube (CNT)	Plastic waste, coal, biomass, hydrocarbon gases.	Chemical Vapor Deposition (CVD), laser ablation, arc discharge, sonochemical, electrolysis	High Mechanical Strength (50–500 G Pa), Electrical Conductivity (3000–3500 W m^{-1} K^{-1}, and Thermal Stability (>700 °C). Diameters from 0.4 to 40 nm.	[70–72]
Graphene Oxide (GO) and Reduced-GO (rGO)	Plastic waste, hydrocarbon gases.	Thermal decomposition, CVD, flash joule heating	High electrical and thermal conductivity (up to ~5000 W m^{-1} K^{-1}), strongest material ever measured (Young's module~1 T Pa), good stretchability, high surface area (theoretical calculations predict a value of 2630 m^2 g^{-1} for monolayer graphene), high chemical and thermal stability.	[68,73]
	Graphite	Electrochemical exfoliation		
Carbon Nitride (g-C$_3$N$_4$)	Triazine and heptazine derivatives, cyanide, urea, melamine.	Solid-state reaction, hard-template method, chemical exfoliation, hydrothermal, thermal decomposition	Tunable optoelectronic properties and metal-free semi-conductor.	[74,75]
Activated Carbon (AC)	Biomass, C-containing wastes (e.g., plastic, food, and agricultural residues), coal, anthracite, peat.	Pyrolysis followed by chemical or physical activation	High surface area (usually s$_{bet}$ >500 m^2 g^{-1}), highly developed internal pore structure, presence of functional groups, especially oxygenated, wide variety of ACS, usually low cost.	[69]

3. Carbon Materials in ODS

The following sections will present the studies related to carbon materials in ODS systems, breaking them into three main sections: (i) hybrid materials containing carbonaceous structures, (ii) carbon-based materials as catalysts on their own, and (iii) systems applying amphiphilic catalysts containing carbon in their structure. As seen in Figure 9, most papers (73%) reported in the literature are related to applying carbon-based materials forming either hybrid materials or as supports for active centers. Fewer papers deal with amphiphilic materials that contain carbon in their structure (15%) or as catalysts on their own (12%).
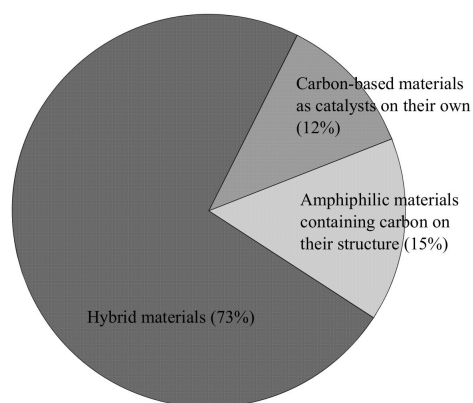
Figure 9. Percentage of published papers regarding the application of (i) hybrid materials containing carbonaceous structures, (ii) carbon-based materials as catalysts on their own, and (iii) systems applying amphiphilic catalysts containing carbon in their structure.

3.1. Carbon Supports and Hybrid Catalysts

One of the advantages of carbon materials is that they can be combined with other materials to prepare composites or hybrid catalysts. Thus, most of the papers related to ODS with carbon materials have applied them in hybrid forms. As discussed before, ODS can be conducted in various systems, such as two-step processes, biphasic systems, under the emulsified form, and solvent-free, among others. Hence, the different systems are separated into different sections.

3.1.1. Two-Step Systems

The papers related to ODS reactions using carbon hybrid materials under a two-step process are gathered in Table 4. As observed, several combinations of hybrid materials consisting of phosphotungstic acid ($H_3PW_{12}O_{40}$, HPW), iron, palladium, molybdenum, and titanium active metal phases with g-C_3N_4, GO and its reduced derivative (rGO), CNTs, and AC as supports/hybrids. The catalytic activities of these hybrid materials have been assessed in ODS of solutions with initial sulfur concentrations ($[S]_0$) ranging from 100 to 9400 ppm using H_2O_2 as oxidant under mild conditions (25–80 °C) and achieving sulfur removals higher than 90%. In general, most authors have not justified the role of the carbon structure in these runs [76–82], with a few exceptions.

Huang et al. (2017) [83] performed ODS of a simulated fuel using dibenzothiophene (DBT) dissolved in n-octane ($[S]_0 = 100$ ppm) using an N-doped onion-like (NOLC) supported HPW. They have obtained high conversions (>90%), which were maintained for up to 10 reuse cycles. They attributed the excellent results to the excellent dispersion of the active phase (HPW) in the NOLC structure. The surface of NOLC displayed a high content of oxygenated groups, which can interact with HPW, strengthening the HPW-support interaction. In turn, the HPW dispersion is improved, boosting the reaction [75]. Rafiee, Shahbazirad, and Khodayari (2017) also found that an increased dispersion of HPW over TiO_2/g-C_3N_4 resulted in higher desulfurization rates of a simulated fuel (DBT ($C_0 = 500$ ppm), BT ($C_0 = 250$ ppm) and Th ($C_0 = 250$ ppm) in EtOH/n-heptane) and for a real oil ($[S]_0 = 500$ or 1900 ppm) [84].

Abdelrahman et al. (2018) [85] also highlighted the high dispersion of Mo_{132} as one of the reasons for the high activity of a hybrid catalyst supported on GO in the ODS of DBT, benzothiophene (BT) or 4,6-dimethyldibenzothiophene (4,6-DMDBT) as model compounds dissolved in dodecane ($[S]_0 = 500$ ppm). They obtained conversions of sulfur compounds higher than 94% regardless of the model compound and were able to maintain the activity up to 10 cycles. Besides the high dispersion of the active phase, GO was also found to increase the adsorption of sulfur compounds due to the Lewis acidic character of its defect sites. The adsorption of sulfur compounds in the catalyst structure approximates the S compound and the oxidant, thus enhancing the oxidation reaction [85].

3.1.2. L-L Biphasic Systems

Tables 5–8 show the studies related to the application of carbon-based hybrid materials in the ODS of a range of sulfur compounds in the biphasic system, i.e., systems where oxidation and extraction occur simultaneously. Each table shows studies using different allotropes of carbon. Not all authors have studied the influence of the carbon structure in the proposed systems [86–89].

Rongxiang et al. (2017) performed ODS of a simulated fuel (DBT in n-octane) using a hybrid catalyst of WO_3 supported over g-C_3N_4. They have found that the most relevant contribution of the carbon structure is related to its high surface area, which in turn allows for a higher dispersion of the active phase [90]. The higher surface area increases the adsorption of sulfur compounds, whereas the higher dispersion impacts the desulfurization performance [90]. The high surface area of AC is also suggested by Xiao et al. (2014) as one of the reasons for the increased activity of HPW supported over AC compared to unsupported HPW in the ODS of thiophene (Th) in a mixed solvent simulating a gasoline matrix [91]. Other authors have also pointed out the high surface area and related high dispersion as relevant contributions of carbonaceous structures to the catalytic activity [92–96]. In contrast, the agglomeration of active centers was linked to a decrease in catalytic activity [97].

Hou et al. (2018) [98], on the other hand, reported that the surface area of the catalyst is not the only relevant parameter for ODS of a simulated fuel (DBT in n-octane) using a g-C_3N_4 supported MoO_2 catalyst. They also observed that the active phase concentration, or loading, is essential information. While increasing the amount of loaded MoO_2 increases the number of active sites, it significantly reduces the surface area of the catalysts, resulting

in poor dispersion of the active sites. On the other hand, low loading of active center results in a catalyst with a high surface area but a low number of active sites. Thus, finding the optimum combination between loading of active phase and maintaining high surface area is a crucial step [98].

In 3D-carbonaceous structures, the surface area was also pointed out as a critical parameter. Ye et al. (2020) have confined MoO_x in a 3D-macroporous carbon structure and applied these hybrid materials in ODS of a simulated fuel (BT, DBT, and 4,6-DMDBT in n-octane). One of the reasons for the high activity of the materials (conversions higher than 85% in 75 min of reaction) was attributed to the high surface area of the 3D-carbon structure, which resulted in a fast mass transfer to the active sites confined within the structure [99]. Zhu et al. (2020) also have observed that the 3D structure of carbon spheres (3D-CS) is beneficial to an increased mass transfer during oxidative desulfurization [97]. Bhadra et al. (2017) also highlighted a fast mass transfer resultant from mesoporosity of the catalyst as an important contributor to the high activity of a TiO_2-C in ODS of a simulated fuel (Th, BT, DBT or 4,6-DMDBT in n-octane, $[S]_0$ = 1000 ppm) [92].

Other authors have pointed out that carbon structures play an important role through adequate adsorption of sulfur compounds, which can be ascribed to an increase in DBT concentration in the vicinity of active catalytic centers [100]. Wang et al. (2010) observed that the main role of CNT in a hybrid catalyst consisting of CNT and a phosphotungstic acid was to enhance the transfer of DBT to the active center by adsorption, facilitating the oxidation of DBT [101]. Xing et al. (2017) observed that increasing the calcination temperature of a $CoWO_4$/g-C_3N_4 resulted in an enhanced surface area and adsorption ability towards DBT [102]. Other authors have also highlighted the adsorption capacity of carbonaceous materials, either towards DBT and other sulfur compounds [90,99,100,103] or towards the oxidation products [104].

Yu et al. (2010) also observed that the adequate adsorption of DBT into the carbon structure was an essential contribution of the carbon-based support in an HPW/AC catalyst [105]. Their reasoning is that increased adsorption of DBT leads to a higher collision probability between DBT and active oxygen species from the decomposition of H_2O_2 that takes place in the active center (HPW). The carbon surface also influences the resonance-stabilization of these active oxygen species, boosting oxidation. Moreover, due to the hydrophobicity of AC, it can be adequately dispersed in the oily phase or placed in the interface between the oily and polar phases, acting as a phase transfer agent [105]. Kermani et al. (2018) also found that the combination between adsorption capacity towards DBT and adequate lipophilicity of AC structure was an essential feature of the composite Mo_{132}/AC [106].

In an ultrasound-assisted ODS (UAODS) of a simulated fuel with an HPW/AC as the catalyst, Liu et al. (2014) also identified the increased adsorption of DBT and the ability of the catalyst to act as a phase transfer agent as important features arising from the AC support [107]. However, they have also pointed out that the AC structure plays another relevant role in UAODS: the high surface area was also correlated to a higher cavitation activity in UAODS, boosting reaction rates [107,108].

Functional groups on the carbon material can impact the coordination of active species (metallic centers) [109–111]. Dini, Afsharpour, and Tabar-Heydar (2019) argued that the oxidation of DBT undergoes an electrophilic attack of the peroxo group (LUMO) on the catalyst surface to the sulfur compound (HOMO) [110]. Thus, efficient oxidation needs to overcome the LUMO-HOMO barrier. The functional groups on the support surface (in this case, CNTs) affect the coordination of the metal-active species (Mo). This geometry boosts the electron density of peroxo groups and increases the HOMO energy level. By increasing the energy level of HOMO, the gap between HOMO-LUMO decreases, and oxidation is facilitated [110,111].

Other authors have correlated the activity of hybrid materials to an increased electron transfer between carbon structure and active phase, especially in doped carbon-based materials. Bhadra, Khan, and Jhung (2019) observed that N-doped graphitic carbon-supported

Co resulted in a more effective electron transfer, which could be helpful for oxidation and reduction reactions [112]. Liao et al. (2019) observed that the strong interaction between HPW and rGO enhanced electron mobility and, consequently, the reaction rate [113].

Wang et al. (2020) [95] and Zhao et al. (2017) [96] have proposed that g-C_3N_4 was able to activate H_2O_2 and form hydroxyl radicals (HO$^\bullet$). Moreover, the carbon structure was also found to avoid the leaching of active species [113].

3.1.3. Other ODS Systems

Table 9 displays a miscellaneous of other ODS systems, whereas Table 10 displays photocatalytic ODS systems. Similar to what was observed earlier, the developed surface area and the structure of pores in carbon materials, leading to well-dispersed active phases, were found as a critical contribution of carbon structures [114–118]. Xun et al. (2020) [119] also highlighted the dispersion of TiO_2 over a graphite carbon (GC) as a relevant factor for the ODS of a simulated fuel (DBT, 4-methyldibenzothiophene (4-MDBT) and 4,6-DMDBT) dissolved in n-octane, $[S]_0$ = 500 ppm). However, they also observed that the dispersion is related to the amount of active phase dispersed on the support. Upon increasing TiO_2 content over 10 wt.%, the catalytic activity of the hybrid catalyst decreased due to the agglomeration of TiO_2 particles. Thus, loading the proper amount of the active phase is an important step. The synergistic effect between the support and the active centers is the main reason a catalyst displays outstanding properties in ODS systems [119]. Gao et al. (2020) [120] found that the increased surface area was also associated with a higher collision probability between sulfur compounds and the catalyst. They observed that the activity of the polyoxometalate-based IL supported over a series of carbon materials decreased accordingly to the surface area of the support (P[C_2VP] MoV/AC (170 m^2 g^{-1}) > P[C_2VP] MoV/CA (157 m^2 g^{-1}) > P[C_2VP] MoV/CNT (93 m^2 g^{-1}) > P[C_2VP] MoV/GO (10 m^2 g^{-1})) [120]. This observation highlights the importance of a developed surface area to a well-dispersed active phase and high desulfurization rates.

Carbon-based materials were also found to accelerate the electron transfer for different active phase-support pair materials, such as MoO_2/g-C_3N_4 [115], FePc (NO_2)$_3$-CF [118], V/P-doped g-C_3N_4 [121], VO-MoO_2@N-doped CNT [122], considering different oxidants (TBHP [115,121], O_2 [118] and CHP [122]), which enhances oxidative desulfurization rate. Chen, Ren, and Yuan (2020) observed that the rate-determining step in the ODS of DBT using V supported over a P-doped g-C_3N_4 material is the electron transfer, and thus an enhanced electron transfer due to P doping greatly improved oxidation [121]. They also observed that P-doping g-C_3N_4 enhanced the electron transfer, resulting in a more efficient ODS process [121].

Some authors have reported that carbonaceous materials favor electron-hole separation [123–127] (cf. Table 10), thus benefiting the photocatalytic activity of those hybrid materials. Li et al. (2017) claimed that the narrower bandgap of g-C_3N_4 allows the application of visible light [124]. Furthermore, the well-matched band structures between support and active phase (CeO_2) favor the ready transfer of electrons generated in the surface of the support to the surface of CeO_2 to avoid the recombination of photo-generated electrons and holes effectively. Thus, the electrons can react with hydrogen peroxide to form hydroxyl radicals. They observed that the holes might also participate in the reaction, although contributing much less than electrons, due to the weak potential of the valence band of g-C_3N_4 (1.79 eV) compared to the redox potential of the OH^-/HO$^\bullet$ pair (1.99 eV) [124]. Ma et al. (2017) also found that the use of carbon quantum dots (CQD) improved the efficiency of the use of visible light [125].

In general, most ODS systems require an extractant phase and a catalyst to remove the oxidized intermediates. However, in a few processes, the hybrid material can act as a catalyst to oxidize sulfur compounds and adsorbents for the oxidized products in a solvent-free approach. Jiang et al. (2017) immobilized a polyoxometalate-based IL in graphite carbon and tested this hybrid catalyst in the solvent-free ODS of a simulated fuel. A 100% removal of DBT in the model oil was observed, whereas only DBT sulfone

(DBTO$_2$) was detected in the catalyst phase. The high efficiency of the process was ascribed to the hydrophilic characteristics of IL, allowing a closer contact with H$_2$O$_2$ associated with the high hydrophobic character of carbon, which allowed a closer contact with the oil phase [128]. Ma et al. (2019) reported similar results. Only DBTO$_2$ was detected in the catalyst phase, and no sulfur compounds were observed in the oil phase [114].

Other reasons pointed out by the authors were the hydrophobic characteristics of GC in a polyoxometalate-based IL supported on GC, which allowed the catalyst to be better dispersed in the oil phase in the solvent-free ODS [128]. The protective environment arising from the CNT structure was also an essential feature, especially to avoid leaching of the active phase, thus increasing catalyst stability and reusability [129].

3.1.4. Trends on Hybrid Materials Containing Carbonaceous Structures

Carbon-based materials have proved to be an exciting platform either as supports for active phases or as components in hybrid materials, leading to highly active catalysts in ODS processes. Carbon materials can be used in a wide range of different approaches and systems. Most authors agree that the main contribution of the carbon-based structure is usually related to the high surface area displayed by those types of materials, which leads to a high degree of dispersion of the active phases. Others have also pointed out that the hydrophobic nature of the carbon structure increases the interaction of the hybrid materials with the organic phase and increases the contact between the oxidant and the target S compound. A few authors also highlighted an increased electron transfer between the carbon structure and the active phase as the critical contribution of carbon structures. Specifically for photocatalytic systems, carbon-based materials have the advantage of reducing the recombination of electron-hole pairs, which dramatically boosts reaction rates. Carbon materials can act as catalysts of the process and adsorb the oxidized compounds, allowing solvent-free systems. Furthermore, carbon materials were able to avoid the leaching of active phases.

3.2. Carbon Catalysts on Their Own

Carbon-based materials have been reported as catalysts on their own for ODS reactions, and a summary with the main conditions and results are collected in Table 11. As observed, a series of carbon-based materials (AC, GO, rGO, and CNT) have been assessed in the ODS of model compounds (mainly BT, DBT, or 4,6 DMDBT). Initial sulfur concentrations ranging between 400 and 2189 ppm were studied, considering mild operating conditions (25–150 °C), allowing to achieve removals higher than 95% from 30 min of reaction time. In general, carbon materials have displayed similar activity to those reported earlier considering hybrid or supported materials. The activity of the carbon material can be ascribed to the presence of defect sites on its surface, its developed surface area, or the presence of surface groups. Here, we propose the mechanism displayed in Figure 10 for the ODS of sulfur-containing compounds according to different proposals in the oxidation activity of carbon catalysts [130,131].

Gonzalez et al. (2012) compared a thermally treated AC (SX-1) and an AC treated with phosphoric acid (MW-99). MW-99 led to an increase in sulfur removal in the range 2.8–3.3 × compared to SX-1, depending on the sulfur compound. Those results were ascribed to a more developed surface area by MW-99, a lower content of basic sites and a higher concentration of acidic sites [132]. Haw et al. (2010) also found that the presence of acidic groups in AC, especially oxygenated groups, increased catalytic activity due to the electron-withdrawing characteristic of the acidic groups allied to the electron donor ability of S compounds. This interaction between acidic groups and S atoms increases the physisorption of S compounds in the AC structure [133].
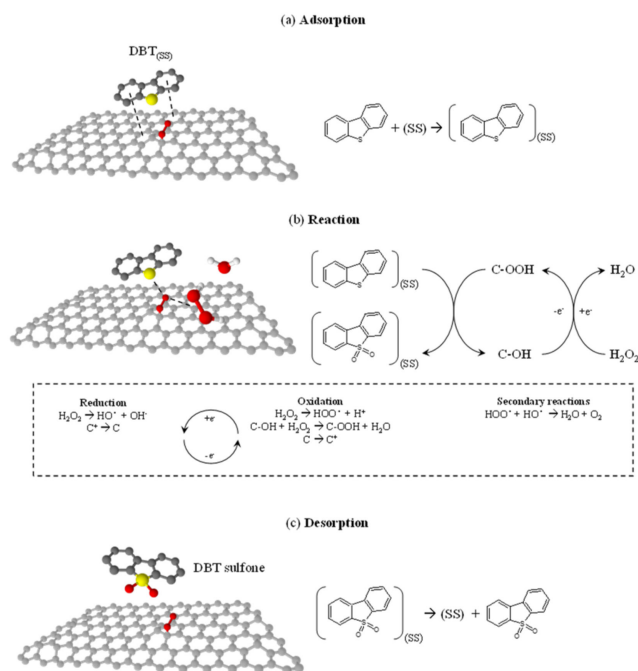
Figure 10. Oxidation mechanism of sulfur compounds (exemplified with DBT) on carbon catalysts (SS = Surface Site, draws prepared with Freeware Chemsketch; White, Red, Yellow, Gray atoms as hydrogen, oxygen, sulfur, and carbon, respectively).

He et al. (2019) [131] studied the influence of doping GO with nitrogen and oxygen for the aerobic ODS of various sulfur compounds. They compared two GO samples. The first was an N-doped GO subjected to annealing at 1000 °C, leading to PG-15. The other sample was obtained by subjecting PG-15 to thermal treatment in a muffle furnace at 450 °C, leading to PG-450. PG-15 removed approximately 9.3% of DBT, which is mainly ascribed to an adsorption effect. On the other hand, PG-450 could remove 98.5% of DBT in 5 h of reaction. The activity of PG-450 was ascribed to the oxygen groups (19.9% as opposed to 3.6% for PG-15) and to an increase in the content of graphitic-like N structure in the material (47.8% in PG-450 vs. 37.2% in PG-15). The main active sites for the activation of O_2 are the oxygenated groups. However, since this activation requires an electron transfer process, the existence of electron-rich oxygenated groups should facilitate this electron transfer. In N, O-doped materials, the existence of electron-rich oxygen groups is ascribed to the enhanced electron delocalization that arises from the N-doping. To demonstrate the synergistic effect of both N and O doping, a graphite material was calcined at 450 °C (Graphite-450) and tested in the ODS reactions. Graphite-450 is rich in oxygenated groups but poor in nitrogenated groups. In 5 h, only a 40% removal of sulfur compounds was observed, thus reinforcing the synergy between N and O doping [131].

The presence of oxygenated groups was also found as crucial by Gu et al. (2019) [134] in the activity of oxidized CNTs (oCNTs). To identify which oxygenated groups were more relevant, they selectively removed different oxygenated groups (carboxylic, lactone, anhydride, phenolic, or carbonyls) through thermal treatment or selectively blocked some of them. When blocking or removing carbonyl groups, the activity of oCNT decreased drastically (from 100% removal of DBT to 31%), thus, pointing out the relevance of carbonyl groups. Gu et al. (2017) [135] have also found a positive correlation between carbonyl groups and catalytic activity. Other authors have reported that lactones and carboxylic groups also play an essential role [130].

On the other hand, some authors have reported that total oxygen-containing groups could not directly correlate to the catalytic activity in ODS experiments [136]. Zhang et al. (2014) have demonstrated that the change in the content of oxygen-containing groups affects the catalytic activity. However, there was no clear correlation between total content

or specific groups in CNTs and desulfurization activity. Nonetheless, they did find a correlation between the increased graphitization degree of CNTs and increased catalytic activity. An increased graphitization is ascribed to a lower degree of defects. They attribute this phenomenon to a higher electron transfer due to higher electrical conductivity in highly graphitic CNTs [136]. In opposition to that, most authors seem to correlate the presence of defect sites to an increase in catalytic activity. Gu et al. (2019) observed an increase in defect sites after acid treatment (D*/G value increased from 1.77 to 1.91 for CNTs and oCNTs, respectively) which were correlated to the increased activity of oCNTs compared to CNTs (along with the oxygenated groups discussed above) [134]. In 2017, Gu et al. [135], by saturating defect sites in rGO through the formation of C-H bonds, have observed a sharp decrease in DBT removal, thus pointing that defect sites also play a significant role in the activity of carbocatalysts. Zeng et al. (2017) [137] also identified zigzag edges and defects in GO as relevant active centers for the catalytic process.

In contrast, Timko et al. (2016) [138] reported that basal plane defects in AC are more relevant than edge defects. They presumed that basal plane defects are oxidized to generate carboxylic or percarboxylic acids on the surface of the material. Those oxygenated groups are then responsible for promoting ODS. The sulfur compounds are also expected to adsorb into the basal planes, increasing local concentration. However, adsorption alone is not sufficient. The surface oxidation allied to an increased local concentration of the sulfur compound in the carbon basal plane is the reason pointed out by the authors that distinguish the activity displayed by distinct ACs [138].

Trends on Carbon-Based Catalysts

In general, there are fewer reports related to the application of carbon-based materials as catalysts on their own in the ODS process as compared to their application in hybrid forms. However, carbon-based materials have proved to be adequate catalysts, and there is still room to study their application for desulfurization purposes.

Overall, the presence of acidic groups on the surface of carbon-based materials was related to higher desulfurization rates due to an acid–base interaction between carbon surface and sulfur molecules. Among the acidic surface groups, oxygen-containing groups are thought to be the active centers by most studies. However, there is still a controversy related to the influence of defect sites in catalytic activity.

Carbon-based materials have some unique advantages, especially their easy manipulation and introduction of surface groups. Nevertheless, there is a lack of reports related to applying doped carbon with heteroatoms other than oxygen and nitrogen. Thus, further investigating the influence of other dopants is an opportunity to apply carbon-based materials as catalysts on their own.

3.3. Amphiphilic Carbons

Amphiphilic carbons are materials that simultaneously display hydrophilic and hydrophobic characteristics. Thus, amphiphilic carbons can better interact with aqueous and organic phases. The contact angle of a water drop onto a material is widely used to describe amphiphilicity. Materials with a contact angle of $0°$ are completely hydrophilic (high water-wettability), whereas materials with contact angles of $180°$ are entirely hydrophobic. Amphiphilicity is an attractive characteristic when considering a biphasic reaction, as is the case of ODS, due to increased contact between an organic phase (fuels) and an extractant phase, which usually presents a more polar nature. Table 12 summarizes the reports related to the application of amphiphilic carbon-based materials for ODS reactions, main operating conditions, and results.

Abdi et al. (2017) [139] studied the removal of DBT from a simulated fuel in a biphasic system using GO/COOH as a catalyst. They have attributed the high removal rates of sulfur to the amphiphilicity of GO/COOH, which allowed for better interaction with both hydrophilic H_2O_2 and hydrophobic sulfur compounds. Similarly, Liu et al. (2020) have observed that POM catalyst alone, due to its hydrophilicity, could not properly contact DBT

(which is lipophilic). Thus, much better interaction between DBT and catalyst was observed by covering the POM catalyst with a hydrophobic carbon layer, significantly increasing the reaction rate [140]. In another approach, Yu et al. (2020) immobilized lipophilic $C_{12}PW$ on hydrophilic g-C_3N_4, thus increasing the utilization of hydrogen peroxide and the contact between DBT and active sites [141].

Li et al. (2019) found that g-C_3N_4 is not only responsible for improving the dispersion of the active phase (BMPO) but also for creating a heterojunction between support and BMPO, which increases the utilization rate of electrons. Furthermore, the amphiphilic character of the catalyst solves the issue with the mass transfer between oily and aqueous phases [142].

Amphiphilic materials can also be applied in PIC-like approaches that rely on emulsion formation. The higher interfacial area between the apolar and polar phases in emulsion systems should increase the reaction rates. Mambrini et al. (2017) have studied ODS of DBT in emulsion systems (cyclohexane/aqueous H_2O_2) using metallic catalysts (Fe and FeMo) modified with carbon to alter their amphiphilicity. Fe and FeMo alone could not remove any DBT; however, stable emulsions were formed when carbon coating was introduced, resulting in increased contact between organic and water phases, thus increasing reaction rates [143]. They proposed that the materials act in two ways: one, by increasing the interfacial area between phases due to the stabilization of an emulsion system, and two, through the activation of hydroxyl species in a Fenton-like system. The generated hydroxyls radicals were then able to oxidize DBT in the interface between the organic and the aqueous phase. The increased polarity and high interfacial area were also responsible for facilitating the extraction of $DBTO_2$ [143]. Figure 11 shows the presumed mechanism for emulsified systems, adapted from elsewhere [144–146]. Other authors have also reported ODS emulsion systems that rely upon amphiphilic catalysts to increase catalytic activity [147].
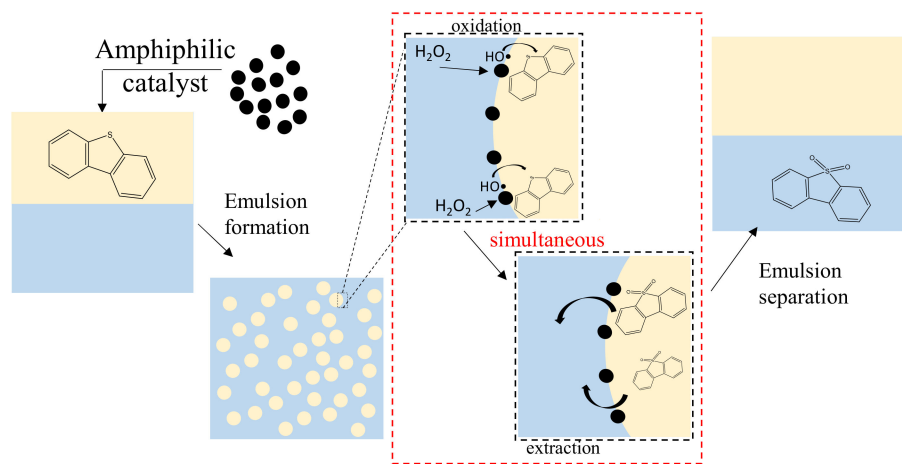
Figure 11. Presumed role of amphiphilic materials in biphasic oxidation under an emulsified system. Adapted from Oliveira et al. (2014) [145], Oliveira et al. (2015) [144], and Teixeira et al. (2013) [146].

Trends on the Application of Amphiphilic Materials

Amphiphilic materials have been applied in an extensive range of different ODS systems, including processes considering two-steps, biphasic systems, and PIC-like approaches. Regardless of the system, amphiphilic materials were attractive options due to their ability to interact with aqueous oxidant phases, lipophilic sulfur compounds, and organic phases simulating fuels.

Table 4. ODS using mainly H_2O with carbon hybrid materials in a two-step system.

Fuel *	Catalyst	Extractant	Operational Conditions	Results	Ref.
DBT in EtOH/Hexane (C_0 = 500–1200 ppm)	$H_5PMo_{10}V_2O_{40}/Fe_3O_4/g$-$C_3N_4$	EtOH	V_{fuel} = 2 mL, m_{cat} = 0.03 g, n_{H2O2} = 10 mmol, T = 80 °C.	Regardless of the initial concentration, complete desulfurization was achieved in 120–180 min. For fuel with $[DBT]_0$ = 1000 ppm, the presence of N compounds slightly hindered the removal of DBT, reducing the overall removal to ~90–95%.	[76]
Real oil ($[S]_0$ = 500 and 1900 ppm)	$H_5PMo_{10}V_2O_{40}/Fe_3O_4/g$-$C_3N_4$	EtOH	V_{fuel} = 5 mL + mixed solvent EtOH: Hexane (1:1, v/v), m_{cat} = 0.03 g, n_{H2O2} = 10 mmol, T = 80 °C.	Twenty five and 30% removal were possible for $[S]_0$ = 500 and 1900 ppm, respectively.	[76]
DBT ($[S]_0$ = 1000–3000 ppm), BT ($[S]_0$ = 100 ppm) or 4,6-DMDBT ($[S]_0$ = 100 ppm) in n-Octane	HPW/mpg-C_3N_4	MeOH	V_{fuel} = 10 mL, m_{cat} = 10–120 mg, H_2O_2/S = 2–12, T = 30–70 °C, t = 0.5–3 h.	DBT: Increasing S content reduced S removal (90, 63, and 58% for $[S]_0$ of 1000, 2000, and 3000 ppm, respectively). In 2.5 h, >99% removal was possible. Increasing the H_2O_2/S ratio from 2 to 4 results in a sharp increase in S removal, followed by a slight increase when further increasing to 8 (100% removal). Maximum desulfurization is achieved at 100 mg of catalyst. Increasing temperature also increases S Removal, especially at lower reaction times. Fifteen recycle runs were possible, maintaining S removals above 98%. Reactivity Followed the Order: DBT~4,6-DMDBT (100%) > BT (80%).	[78]
DBT (C_0 =500 ppm), BT (C_0 = 250 ppm), and Th (C_0 = 250 ppm) in EtOH/n-Heptane	HPW-TiO_2/g-C_3N_4	DMF	V_{fuel} = 5 mL, m_{cat} = 0.03 g, n_{H2O2} = 12 mmol, T = 80 °C.	100% removal of S compounds in 3 h of reaction was observed. In the presence of aromatic or N compounds, 100% removal was also possible but with longer reaction times (4–6 h).	[84]
Real Oil ($[S]_0$ = 500 or 1900 ppm)	HPW-TiO_2/g-C_3N_4	DMF: n-heptane (1:1 v/v)	V_{fuel} = 5 mL, V_{DMF} = 5 mL, m_{cat} = 0.03 g, n_{H2O2} = 12 mmol, T = 80 °C, t = 200 min.	Thirty and 35% decrease in S content was observed ($[S]_0$ of 500 and 1900 ppm, respectively).	[84]
Naphtha ($[S]_0$ = 870 ppm)	Pd/CNTs	ACN	C_{cat} = 0–8.5 g mL^{-1}, Volume Ratio Fuel/ H_2O_2 = 10, T = 25 °C, t = 30 min.	Increasing the catalyst dosage from 2.5 to 8.5 g mL^{-1} resulted in a sharp increase in S removal (25 to 90%, respectively).	[77]
Naphtha (C_0 = NM)	MnO_x/CNT	ACN	C_{cat} = 5 mg mL^{-1}, V_{H2O2} = NM, T = 25–30 °C, t = 30 min.	After 30 min, comparing EDS and ODS process, desulfurization of 9 and 83% were achieved, respectively. Under optimum conditions, 92% desulfurization was observed, maintained for 4 cycles.	[79]
Gas Oil ($[S]_0$ = 9400 ppm)	Fe_2O_3-GO	ACN	V_{fuel} = 100 mL, m_{cat} = 0.5–2.5 g, V_{H2O2} = 10 mL, 5 mL of acetic acid, T = 40–60 °C, t = 160–240 min, 2 g of Na_2CO_3 in 20 mL of Water to Stop the Reaction.	A DoE was used to determine the importance of some parameters, which were found to be: time > temperature > catalyst dosage. The optimum desulfurization (92%) was predicted at 225 min of reaction, 2.5 g of catalyst, and 60 °C.	[81]

Table 4. *Cont.*

Fuel *	Catalyst	Extractant	Operational Conditions	Results	Ref.
DBT, BT, or 4,6-DMDBT in Dodecane ($[S]_0$ = 500 ppm)	Mo_{132}/GO	ACN	C_{cat} = 1–10 g L^{-1}, Molar Ratio H_2O_2/DBT = 2–8, T = 30–60 °C, t = 45–150 min.	DBT: Increasing reaction time results in higher removal of S (48% at 45 min vs. 96% at 150 min). Increasing the H_2O_2/S Ratio over 6 did not impact S removal. Temperature also slightly influenced (96 to 99% from 30 to 60 °C, respectively). Increasing catalyst concentration (1 to 10 g L^{-1}) improved S removal. S removal was ~96 and 94% for 4,6-DMDBT and BT, respectively. Up to 10 recycle runs, a variation of about 1 ppm in the final S content is observed.	[85]
DBT in n-Octane ($[S]_0$ = 500 ppm)	CoMo/rGO	ACN	V_{fuel} = 50 mL, m_{cat} = 0.32 g, V_{H2O2} = 0.3 mL, T = 60 °C.	A 55–99% conversion of DBT depending on reaction conditions. The catalyst could be reused 10 times.	[148]
Commercial Diesel ($[S]_0$ = 440 ppm)	Ce/Fe-AC	DMF	V_{fuel} = 10 mL, T = 45 °C, t = 30 min. (Oxidant = TBHP)	Final S content decreased to 38 ppm.	[149]
Hydrotreated Gas Oil Sample ($[S]_0$ = 1477 ppm)	Pd or Fe_2O_3/AC	ACN	V_{fuel} = 100 mL, m_{cat} = 3 g, V_{H2O2} = 10 mL, T = 40 °C, t = 3 h, 5 mL of Acetic Acid and 2 g Na_2CO_3 (Co-Catalysts) in 20 mL (Dropwise Addition).	Different systems were compared. When using only H_2O_2 and no co-catalyst, 10–12% desulfurization rates were achieved. By adding acetic acid and Na_2CO_3, 71 and 66% desulfurization efficiency was observed for Fe_2O_3/AC and Pd/AC, respectively.	[80]
DBT, BT, and Th in EtOH/n-Heptane (1:1 v/v) ($[S]_0$ = 250–1000 ppm)	C@ $H_5PMo_{10}V_2O_{40}$	Et_2O	V_{fuel} = 5 mL, m_{cat} = 1.4 × 10^{-4} g, V_{H2O2} = 8 µL.	Removal of 90, 86, and 60% was observed depending on $[S]_0$ (250, 500, and 1000 ppm, respectively).	[82]
Light Cycle Oil (LCO) ($[S]_0$ = 530 ppm)	C@$H_5PMo_{10}V_2O_{40}$	DMF	V_{fuel} = 5 mL + 5 mL of Solvent EtOH: n-Heptane (1:1 v/v), m_{cat} = 1.5 × 10^{-4} g, V_{H2O2} = 8.5 µL	A 76% reduction of sulfur was observed.	[82]
DBT in n-Octane ($[S]_0$ = 100 ppm)	HPW/NOLC	MeOH	V_{fuel} = 10 mL, C_{cat} = 2–10 g L^{-1}, H_2O_2/S = 2–10, T = 30–80 °C, t = 0.5–3 h.	Increasing HPW loading (5–10%): Higher S Removal (95–100%, respectively). S removal reached saturation with a 2 h reaction time (at C_{cat} = 4 g L^{-1}). Increasing H_2O_2/S ratio (2 to 6): Sharp improvement in S removal, a further increase to 8 results in complete S removal. Increasing temperature (30 to 40 °C): a sharp increase in S removal. Further increasing to 60 °C allows complete S conversion. At 80 °C, a slight decrease in S removal was observed. Over 90% conversion of DBT was maintained for 10 cycles.	[83]

* If the model fuel is described using the word 'and', it means the model fuel was a mixture of the sulfur compounds. The word 'or' indicates that the sulfur compounds were used independently. *Legend*: NM = not mentioned. AC = activated carbon. ACN = acetonitrile. CNT = carbon nanotube. DMF = dimethylformamide. EtOH = ethanol. Et_2O = diethyl ether. g-C_3N_4 = graphitic carbon nitride. GO = graphene oxide. HPW = phosphotungstic acid ($H_3PW_{12}O_{40}$). MeOH = methanol. mpg-C_3N_4 = mesoporous graphitic carbon nitride. NOLC = N-doped onion-like carbon.

Table 5. ODS using H_2O_2 as oxidant with hybrid materials based in carbon nanotubes (CNTs), graphene oxide (GO), and reduced GO (rGO) in an L-L biphasic media.

Fuel	Catalyst	Extractant	Operational Conditions	Main Results	Ref.
DBT, BT or 4,6-DMDBT in n-Octane ($[S]_0 = 800$ μg g^{-1})	WO_3/CNT	ACN	V_{fuel} = 5 mL, V_{ACN} = 1 mL, m_{cat} = 0.03 g, H_2O_2/S = 5, T = 50 °C, t = 60 min.	Removals of ~78, 90, and 85% were observed for BT, DBT, and 4,6-DMDBT, respectively. dbt conversion was maintained for 4 cycles, in the 5th run decreasing to 80%.	[86]
DBT, 4,6-DMDBT, 2-MBT, 3-MBT, 3-MTh in n-Octane ($[S]_0 = 2.8$ mg mL^{-1})	CNT/PVP/MTO	ACN	V_{fuel} = 2 mL, Molar Ratio Fuel/ACN = 3:1, n_{cat} = 0.1 mmol, 4 Equivalents of H_2O_2, T = 60 °C, t = 24 h.	The order of reactivity was DBT >4,6-DMDBT >2-MBT~3-MBT >3-MTh. Conversion of all sulfur compounds was higher than 99%. After the 6th recycle run, conversion dropped to around 40–78% (depending on the compound) and stabilized around 40–70% up to the 10th run. On the other hand, yield towards the respective sulfones varied between 38–99% depending on the S compound.	[109]
DBT in n-Octane (C_0 = 100–500 ppm)	NH_2/COOH-CNT /MoO_3	ACN	V_{fuel} = 4 mL, V_{ACN} = 2 mL, m_{cat} = 2.5–7.5 mg, H_2O_2/S = 0.5–2, T = 25–60 °C.	With no extraction solvent, removal rates were low. The best desulfurization was observed at 60 °C, 7.5 mg of Catalyst, H_2O_2/S ratio of 2, Resulting in 99% desulfurization. Increasing sulfur concentration slightly decreased conversion to 98%.	[110]
DBT ($[S]_0$ = 100–600 ppm), BT ($[S]_0$ = 300 ppm), or 4,6-DMDBT ($[S]_0$ = 300 ppm) in n-Octane	WO_3/MoO_3-CNT	ACN	V_{fuel} = 5 mL, V_{ACN} = 1 mL, n_{cat} = 0.1–0.3 mmol, V_{H2O2}= 0.5–1.5 mL, T = 25–60 °C.	Ninety nine percent conversion of DBT for $[S]_0$ = 100 or 300 ppm, which drops to 95% when $[S]_0$ =600 ppm. The maximum conversion of BT is 99%, whereas 4,6-DMDBT is 82%. Conversion depends on the initial concentration of precursors.	[111]
DBT in n-Hexane ($[S]_0$ = 521 ppm)	W/CNT	ACN	V_{fuel} = 20 mL, V_{ACN} = 10 mL, C_{cat} = 5 g L^{-1}, H_2O_2/S = 17, T = 10–50 °C, t = 90 min.	At room temperature, a conversion higher than 95% was obtained. After the 4th recycle run, conversion dropped to 25% due to poisoning of active sites.	[103]
DBT in n-Octane ($[S]_0$ = 100–1100 ppm)	$Cs_{2.5}H_{0.5}PW_{12}O_{40}$/CNT $Cs_{2.5}H_{0.5}PW_{12}O_{40}$/AC	ACN	V_{fuel} = 60 mL, V_{ACN} = 60 mL, m_{cat} = 1 wt.% (in Relation to Fuel), H_2O_2/S = 20, T = 60 °C, t =160 min.	Using CNT as support increased sulfur removal from 90 to 100%, Compared to AC support. A 100% conversion of dbt was obtained and 100% yield towards the sulfones. Three cycles were run with only a slight decline in conversion.	[101]
DBT in n-Octane ($[S]_0$ = 320 ppm)	HPW/rGO	MeOH	V_{fuel} = 15 mL, V_{MeOH} = 10 mL, m_{cat} = 0.1–0.25 g, H_2O_2/S = 2–8, T = 60 °C.	Increasing catalyst load over 0.2 g does not have a significant effect on desulfurization. The best H_2O_2/S Ratio was 8. 95% of DBT was converted in 8 h and maintained for 5 cycles.	[113]
Th, BT, DBT, 4-MBT, or 4,6-DMDBT in n-Octane (C_0 = 2000 ppm)	[Vim]POM/GO [DVim]POM/GO P[Vim]POM/GO	DMF	V_{fuel} = 10 mL, V_{DMF} = 10 mL, m_{cat} = 0.1 g, V_{H2O2}= 0.56 mL (H_2O_2/S = 9), T = 50 °C.	Desulfurization efficiency of the IL were: P[Vim]POM (100%, for 5 runs) > [Vim]POM (93%) > [DVim]POM (86%) for DBT. Removals for the remaining S compounds: 4,6-DMDBT and 4-MBT were 100% and BT and Th were 96% and 92%, respectively.	[87]
DBT, BT, or 4,6-DMDBT ($[S]_0$ = 500 ppm, each) in n-Hexane and a Mixed Fuel of DBT, BT, and 4,6-DMDBT ($[S]_0$ = 500 ppm, Total) in n-Hexane	HPW/GO	ACN	V_{fuel} / V_{ACN} = 1, C_{cat} = 5 g L^{-1}, H_2O_2/S = 6, T = 60 °C.	DBT and 4,6-DMDBT removal achieved 100%, whereas BT was only 70%. In mixed fuel, overall S removal was 99%. Removal of S higher than 90% for 8 cycles.	[150]
DBT, BT, or 4,6-DMDBT in n-Hexane ($[S]_0$ = 500 mg g^{-1})	$H_3PMo_{12}O_{40}$-GO	ACN	V_{fuel} = 5 mL, V_{ACN}/V_{fuel} = 0.1–1, C_{cat} = 1–3 g L^{-1}, H_2O_2/S = 2–8, T = 25–60 °C.	BT removal varied from 55–70%, DBT 70–100%, and 4,6-DMDBT 70–100%, depending on operational conditions. Optimal operating conditions were 50 °C, $V_{extractant}$/V_{fuel} of 0.3 and H_2O_2/S of 6.	[151]

Legend: AC = activated carbon. ACN = acetonitrile. DMF = dimethylformamide. [DVim] = cation from the IL 113divinyl-3-decyl diimidazolium bromide. PVP = poly(4-vinyl pyridine). HPW = phosphotungistic acid ($H_3PW_{12}O_{40}$). MeOH = methanol. MTO = Methyltrioxorhenium. POM = polyoxometalate ($H_8P_2Mo_{16}V_2O_{62}\cdot14H_2O$). [Vim] = cation from the IL 1-vinyl-3-amylimidazolium bromide.

Table 6. ODS using H_2O_2 as oxidant with hybrid materials based on activated carbon (AC) in an L-L biphasic media.

Fuel	Catalyst	Extractant	Operational Conditions	Main Results	Ref.
Th in a Mixed Solvent (Xylene, Octadiene, Cyclohexene, n-Hexane) ($[S]_0$ = 489 ppm)	HPW/AC	H_2O_2 Aqueous Solution	V_{fuel} = 20 mL, m_{cat} = 0.5 g, V_{H2O2} = 4 mL, 0.05 g of CTAB, Emulsified System.	In simulated fuel using only n-Hexane, desulfurization of 90% was obtained at 90 °C and 120 min. For mixed solvents, upon adding 1–15 wt.% of xylene, Th removal was 75.9–59.2%. Similarly, for cyclohexane addition (1–15 wt.%), a Th Removal of 62–7% was observed. Adding Octadiene (1–15 wt.%) decreased Th conversion to 52.6–31.4%. Octadiene and Cyclohexane have a strong negative effect, whereas Xylene has a milder negative effect.	[91]
Commercial Gasoline ($[S]_0$ = 280 ppm)	HPW/AC	H_2O_2 Aqueous Solution	V_{fuel} = 20 mL, m_{cat} = 0.5 g, V_{H2O2} = 4 mL, 0.05 g of CTAB, Emulsified System.	Sulfur removal depended greatly on the compound. Th desulfurization was only 32%.	[91]
DBT in n-Octane (C_0 = 2000 ppm)	HPW/AC	H_2O_2 Aqueous Solution	V_{fuel} = 40 mL, Mass Ratio Cat: Fuel = 1.25:100, vol. ratio H_2O_2: Fuel = 1:10, T = 60 °C, t = 12 min, 70 W.	Decreasing particle size of the AC support improves desulfurization due to an increase in surface area. Increasing HPW loading up to 10% increases desulfurization; however, further increasing reduces AC surface area and interferes with the ac structure effect in the ultrasound-assisted process. Ultrasound power over 70 W did not improve desulfurization. DBT removal was 100%.	[108]
Th in n-Octane (C_0 = 656 ppm)	Pd/AC	Aqueous Solution Containing 2 g NaOH, 5 g Water, and 2.5 g 2-Propanol	m_{fuel} = 14 g, $m_{extractant}$ = 9.5 g, m_{cat} = 0.05 g, $m_{oxidant}$ = 2.5 g (2-Propanol), T = 50–70 °C, In-Situ Generation of H_2O_2 from 2-Propanol.	After 20 min at 70 °C, a model fuel with sulfur content lower than 1 ppm is obtained. Obtaining fuels with ultra-low sulfur at lower temperatures is possible; however, more time is required. >99% conversion was maintained for 5 cycles.	[104]
DBT in n-Octane (C_0 = 2000 ppm)	HPW/AC	H_2O_2 Aqueous Solution	V_{fuel} = 40 mL, C_{cat} = 1.25 wt.%, Volume Ratio H_2O_2: Fuel = 1:400–1:10 (H_2O_2/S = 3–123), T = 40–70 °C, t = 3–30 min, 70–100 W Ultrasound, Emulsion Formation.	Upon increasing HPW loading, the reaction rate increased up to a 10 wt.% loading. increasing catalyst concentration also improves desulfurization (up to 1.25 wt.%), whereas higher catalyst loading hinders the propagation of ultrasound waves. Comparing the ultrasound-assisted process to a regularly mixed process, ultrasound resulted in a 30% improvement. Temperature played a very significant role in increasing the reaction rate. At 40 °C, 70% of DBT is oxidized in 30 min, whereas at 70 °C, 100% is oxidized in 9 min. The proper amount of oxidant was important to fully wet the carbon surface and to permit emulsion formation. Desulfurization decreased to 90% and ~75% in the 2nd and 3rd runs, respectively.	[107]
DBT in n-Octane ($[S]_0$ = 300 ppm)	HPW/AC	H_2O_2 Aqueous Solution	m_{fuel} = 25 g, m_{cat} = 0.1 g, H_2O_2/S = 4, T = 80 °C, t = 40 min.	HPW Loading of 10% was found as optimal. Increasing the H_2O_2/S Ratio and temperature improves desulfurization. At lower temperatures, a higher amount of oxidant is necessary to achieve full desulfurization. A total of 100% removal of DBT obtained.	[105]
DBT in n-Octane ($[S]_0$ = 500–1000 ppm)	Mo$_{132}$/AC	ACN	V_{fuel} = 5 mL, V_{ACN} = 5 mL, m_{cat} = 0–0.005 g, H_2O_2/S = 2–30, T = 25–45 °C.	With no catalyst, 46% removal of DBT was observed in 120 min. Using 0.0025 g of catalyst Led to 100% removal in 30 min. Temperature shortened reaction time required to achieve deep desulfurization to 10 min at 45 °C. Increasing the H_2O_2/S ratio improved desulfurization up to 10, further increase negatively affected s removal. A total of 100% removal was achieved for $[S]_0$ of 500, 700, and 1000 in 30, 60, and 120 min.	[106]

Legend: ACN = acetonitrile. HPW = phosphotungistic acid ($H_3PW_{12}O_{40}$).

Table 7. ODS using mainly H_2O_2 with hybrid materials based on other carbon forms in an L-L biphasic media.

Fuel	Catalyst	Extractant	Operational Conditions	Main Results	Ref.
Th, BT, DBT, or 4,6-DMDBT in n-Octane ($[S]_0$ = 1000 ppm)	TiO_2-C	ACN	V_{fuel} = 10 mL, V_{ACN} = 5 mL, m_{cat} = 20 mg, V_{H2O2}= 0.114 mL (H_2O_2/S = 15), T = 80 °C.	The reactivity order is DBT (100%) > BT (60%) > Th (50%) > 4,6-DMDBT (38%). For DBT model fuel, conversion >95% was maintained for 5 runs.	[92]
Th in n-Heptane (C_0 = 300 ppm)	MoO_2/C	IL: [Hnmp]BF_4	V_{fuel} = 20 mL, V_{IL} = 3 mL, m_{cat} = 0.1 g, V_{H2O2}= 2 mL, T = 70 °C.	Upon increasing IL and H_2O_2, higher Th removal was observed. Temperature played a very relevant role: removals of >95% (70 °C), 65% (60 °C), 50% (50 °C) and <20% (40 °C) in 240 min were observed.	[88]
Th, BT or DBT in n-Octane ($[S]_0$ = 1000 ppm)	W_2N/C	ACN	V_{fuel} = 10 mL, V_{ACN} = 5 mL, m_{cat} = 0.02 g, H_2O_2/S = 15, T = 30–80 °C.	DBT conversion maintained over 90% for 5 cycles. Removals of Th and BT were 80 and 90%, respectively.	[93]
DBT in Hexane (C_0 = 1000 ppm)	PET-Modified Red Mud	ACN	V_{fuel} = 10 mL, V_{ACN} = 2 mL, m_{cat} = 5–20 mg, V_{H2O2}= 1 mL, T = 25 °C.	Maximum removal of 80% is observed at a catalyst loading of 10 mg. Exceeding that value does not improve desulfurization.	[94]
BT, DBT or 4,6-DMDBT in Heptane (C_0 = 0.5 mmol)	$H_3PMo_{12}O_{40}$/C	H_2O	V_{fuel} = 5 mL, $V_{extractant}$ = 5 mL, n_{cat} = 0.0041 mmol, n_{H2O2}= 1.5 mmol, H_2O_2/S = 3, T = 60 °C.	A 100% conversion of DBT in 30 min for 8 Cycles. 4,6-DMDBT required 60 min to be degraded, whereas BT Required 120 min. Increasing H_2O_2/S over 3 impacted the efficiency of H_2O_2 use. Increasing reaction temperature over 60 °C negatively affected the reaction.	[100]
Pyrolysis Oil of Waste Tires ($[S]_0$ = 7139 ppm)	Biochar	Aqueous 10 wt.% H_2O_2 Phase	m_{fuel} = 2 g, $V_{extractant}$ = 15 mL, $V_{10wt.\%\ H2O2}$ = 15 mL, T = 60–100 °C, t = 2–6 h.	Desulfurization ranged from 33–64% depending on catalyst concentration and on the precursor of the biochar (coffee ground or waste tire).	[152]
DBT, Th, BT, or 4,6-DMDBT in n-Octane (C_0 = 1000 ppm)	Co/N-doped C	ACN	V_{fuel} = 20 mL, V_{ACN} = 5 mL, m_{cat} = 10 mg, V_{H2O2} = 0.2 mL, H_2O_2/S ratio = 15, T = 70 °C, t = 120 min.	~93% removal of DBT for 5 cycles. Removals of BT, Th, and 4,6-DMDBT were 65, 50, and 50%, respectively.	[112]
DBT, 4-MDBT or 4,6-DMDB in Dodecane ($[S]_0$ = 200 ppm)	HPW/3D-CS	Adsorption on 3D-CS	V_{fuel} = 5 mL, 1 mL of acetic acid, m_{cat} = 0.2 g, H_2O_2/S = 8, T = 70 °C, t = 40 min.	The optimal loading of HPW was found to be 7 wt.%. A total of 100% removal of DBT maintained for 3 cycles, slight decrease on the 4th and 5th cycles (to 93%). the desulfurization rate was very similar regardless of the model sulfur compound. One hundred percent desulfurization was achieved for all model oils in 2.5 h.	[97]
Th in n-Octane ($[S]_0$ = 1000 ppm)	[C_nVP]MoV/ CA (n = 2, 4, 6, 8, or 10)	DMF	V_{fuel} = 40 mL, V_{DMF} = 10 mL, m_{cat} = 0.04 g, O_2 flow rate 1 L min^{-1}, T = Room Temperature.	Increasing the chain length of the catalyst (n = 2–6) increases desulfurization. For n > 6, the steric hindrance of the material increases, and desulfurization is hindered. The maximum removal observed was 99.6%.	[89]

Legend: ACN = acetonitrile. CA = carbon aerogel. CS = carbon spheres. [C_nVP] = cation from the IL N-alkyl-4-vinylpyridinium bromide. DMF = dimethylformamide. IL = ionic liquid. MoV = heteropoly acid substituted by vanadium ($H_8P_2Mo_{16}V_2O_{62}$).

Table 8. ODS using H_2O_2 with hybrid materials based on graphitic carbon nitride (g-C_3N_4) in an L-L biphasic media.

Fuel	Catalyst	Extractant	Operational Conditions	Main Results	Ref.
BT, DBT, or 4,6-DMDBT in n-Octane ($[S]_0 = 320$ ppm)	MoO_3/g-C_3N_4	MeOH	$V_{fuel} = 15$ mL, $V_{MeOH} = 15$ mL, $C_{cat} = 0.013$ mg L^{-1}, $H_2O_2/S = 4$, T = 60 °C.	With the addition of specific scavengers for $\bullet O_2^-$, h^+, e^- and $HO^\bullet$, the authors have observed that $HO^\bullet$ was the most important radical. desulfurization rates were: >96% removal for 6 cycles (DBT), >85% for 4,6-DMDBT and 60% for BT.	[95]
DBT, BT or Th in n-Octane ($[S]_0 = 500$ µg g^{-1})	WO_3/g-C_3N_4	IL: 1-Ethyl-3-Methylimidazolium Ethyl Sulfate	$V_{fuel} = 5$ mL, $V_{IL} = 1$ mL, $m_{cat} = 0.02$ g, $V_{H2O2} = 0.2$ mL, T = 70 °C, t = 3 h.	WO_3 supported over g-C_3N_4 has a higher desulfurization activity than unsupported WO_3 or supported over alumina. The order of reactivity was DBT (96%) > BT (73%) > Th (53%). The catalyst could be reused 5 times with >85% removal of DBT.	[90]
DBT, BT or Th in n-Octane ($[S]_0 = 500$ µg g^{-1})	$CoWO_4$/g-C_3N_4	IL: [EMIM][EtSO_4]	$V_{fuel} = 5$ mL, $V_{IL} = 1$ mL, $m_{cat} = 0.03$ g, $V_{H2O2} = 0.4$ mL, T = 80 °C, t = 180 min.	DBT was easily removed, achieving over 90% conversion, maintained for 5 cycles. BT and Th maximum removals were 40%.	[102]
DBT, 4,6-DMDBT or Th in n-Octane ($[S]_0 = 500$ µg g^{-1})	MoO_2/g-C_3N_4	IL: [BMIM][BF_4]	$V_{fuel} = 5$ mL, $V_{IL} = 0.5$–1.5 mL, $m_{cat} = 0$–0.03 g, $V_{H2O2} = 0$–0.2 mL, T = 50–80 °C.	Increasing loading of MoO_2 to 3 wt.% resulted in higher desulfurization. A 5 wt.% loading negatively affected the S removal. Temperatures higher than 60 °C, catalyst dosage over 0.02 g, and IL volume higher than 1 mL resulted in lower desulfurization performances. Maximum removal was observed with 0.2 mL of oxidant. Maximum conversions were 95% (DBT, 120 min), 60% (4,6-DMDBT, 140 min) and 35% (Th, 140 min).	[98]
BT, DBT, or 4,6-DMDBT in n-Octane ($[S]_0 = 800$ ppm)	MoO_x@3D-g-C_3N_4	Methyl cyanide	$V_{fuel} = 30$ mL, $V_{extractant} = 6$ mL, $m_{cat} = 0.005$–0.01 g, $m_{H2O2} = 0.15$ g ($H_2O_2/S = 5$), T = 0–60 °C, t = 75 min.	Maximum desulfurization was 100% for DBT, 91% for BT and 91% for 4,6-DMDBT.	[99]
DBT, BT or Th in n-Octane ($[S]_0 = 500$ ppm)	WO_3/g-C_3N_4	IL: 1-Ethyl-3-Methylimidazolium Diethylsulfate	$V_{fuel} = 5$ mL, $V_{IL} = 0.25$ mL, $m_{cat} = 0.03$ g, $V_{H2O2} = 0.3$ mL, T = 60 °C, t = 180 min.	Increasing WO_3 loading to 36% results in an increase in desulfurization. With 50% loading, the desulfurization was negatively affected. A 90% conversion for DBT was observed (150 min) and maintained for 5 cycles. Th Removal of 60% was observed regardless of reaction time (20–180 min), and for BT a maximum of 43% was obtained in 180 min.	[96]

Legend: IL = ionic liquid. MeOH = methanol.

Table 9. Other ODS systems with carbon-based hybrid materials.

Fuel	Catalyst	Oxidant	Extractant	Operational Conditions	Main Results	Ref.
DBT in n-Octane ($[S]_0$ = 2000 ppm)	CNT@PPDA@$H_8P_2Mo_{16}V_2O_{62}$	O_2	N.M.	V_{fuel} = 100 mL, C_{cat} = 1 g L^{-1}, 1.5 L min^{-1} of O_2, T = 70 °C.	Using a DoE, the temperature was the most relevant variable, followed by catalyst mass and oxygen quantity. Conversion of DBT was maintained above 95% up to 8 cycles.	[153]
DBT in n-Octane ($[S]_0$ = 2000 ppm)	CNT@MOF-199-$H_8P_2Mo_{16}V_2O_{62}$	O_2	N.M.	V_{fuel} = 50 mL, m_{cat} = 0.1 g, 1.5 L min^{-1} O_2 flow, T = 60 °C.	~100% DBT Removal in 180 min. >90% conversion maintained for 7 cycles.	[154]
DBT, 4-DMDBT or 4,6-DMDBT in n-Octane ($[S]_0$ = 2000 ppm)	P[C_2VP] Br/AC, P[C_2VP] Br/CA, P[C_2VP] Br/CNT, P[C_2VP] Br/GO	O_2	N.M.	V_{fuel} = 50 mL, 15 μmol of the active phase of catalyst, 1.5 L min^{-1} of O_2, T = 70 °C.	Activity in the order: P[C_2VP] Br/AC > P[C_2VP] Br/CA > P[C_2VP] Br/CNT > P[C_2VP] Br/GO, which agrees with the surface area of the catalysts. A total of 99.2% removal of DBT maintained for 5 cycles. On the 6th cycle, desulfurization decreases to 95% and on the 8th to 90%. 4-MDBT and 4,6-DMDBT conversions were 95 and 80%, respectively.	[120]
DBT or 4,6-DMDBT in n-Octane ($[S]_0$ = 500 ppm)	VO-MoO$_2$@N-doped CNT	CHP	N.M.	V_{fuel} = 15 mL, m_{cat} = 0.08 g, CHP/S = 4, T = 70 °C, t = 1 h.	A 100% removal was attained for both S compounds. For The oxidation of 4,6-DMDBT, 4 recycle runs were possible with no change in conversion. From the 5th run, a linear decrease was observed up to the 8th run (which resulted in 80% conversion).	[122]
DBT, 4-MDBT, or 4,6-DMDBT in Dodecane ($[S]_0$ = 200 ppm)	[(C_8H_{17})$_3$NCH$_3$]$_3$H$_3$V$_{10}$O$_{28}$/3D-g-C_3N_4	Air (O_2)	Oxidized compounds were removed in the catalyst phase.	V_{fuel} = 20 mL, m_{cat} = 0.01 g, 100 mL min^{-1} air flow, T = 120 °C.	In 6 h of reaction, >95% of S was removed, regardless of the S compound tested, leading to fuel with <10 Ppm S content (for 5 cycles). Adding 5 Wt.% of Cyclohexane and P-Xylene slowed the reaction rate; however, it was still possible to achieve deep desulfurization in 8 h of reaction.	[117]
DBT, 4-MDBT, 4,6-DMDBT, or 3-MBT in n-Octane ($[S]_0$ = 500 ppm)	WO$_3$/few-layer g-C_3N_4	H_2O_2	Oxidized compounds were removed in the catalyst phase.	V_{fuel} = 5 mL, m_{cat} = 0.05 g, H_2O_2/S = 3, T = 50 °C, t = 40 min.	A 100% removal for up to 6 runs (DBT). One hundred percent removal in 60 min was obtained for all sulfur compounds; however, kinetics were distinct (DBT >4-MDBT >4,6-DMDBT >3-MBT).	[114]
DBT in Decalin (C_0 = 500 ppm)	MoO$_2$/g-C3N4	TBHP	N.M.	m_{fuel} = 10 g, m_{cat} = 0.05 g, m_{TBHP} = 0.1141 g (TBHP/S = 3), T = 80 °C, t = 2 h.	A 100% removal Of DBT. Hydroxyl radicals (HO•) and electron (E$^-$) are the main active species in DBT oxidation, followed by •O_2^-.	[115]
DBT ($[S]_0$ = 500 ppm) and 4,6-DMDBT ($[S]_0$ = 250 ppm) in n-Octane	[(C_6H_{13})$_3$PC$_{14}$H$_{29}$]$_3$PMo$_{12}$O$_{40}$/g-C_3N_4	H_2O_2	Adsorption on g-C_3N_4.	V_{fuel} = 5 mL, m_{cat} = 0.05 g, H_2O_2/S = 4, t = 180 min.	>93% of removal of DBT and >90% of 4,6-DMDBT maintained for 6 cycles.	[116]
DBT, 4,6-DMDBT or BT in n-Octane (C_0 = 500 ppm)	V/P-doped g-C_3N_4	TBHP	N.M.	V_{fuel} = 30 mL, m_{cat} = 0.02 g, m_{TBHP} = 0.0313 g, T = Room Temperature-60 °C.	A 100% DBT removal in 60 Min. Over 80% removal was maintained For 5 Cycles. BT and 4,6-DMDBT removals were 80 And 75%, respectively.	[121]

Table 9. *Cont.*

Fuel	Catalyst	Oxidant	Extractant	Operational Conditions	Main Results	Ref.
DBT in n-Hexane ($[S]_0$ = 500 ppm) and mixed fuel of BT, DBT, and 4,6-DMDBT ($[S]_0$ = 125 ppm, each) in n-Octane	MoO_2@GNF	TBHP	N.M.	V_{fuel} = 5 mL, m_{cat} = 5 mg, V_{TBHP} = 0.14 mL, T = 60 °C, t = 120 min. Solvent-Free.	The synthesized catalyst acts as a Nanosponge for the oxidized compounds; no extractant is required. Desulfurization achieved values >95% for all components resulting in a final S content of 6.5 ppm.	[129]
DBT, 4-MDBT, and 4,6-DMDBT in Dodecane ($[S]_0$ = 200 mg kg^{-1})	MoO_x/MC	O_2	Adsorption in the catalyst.	V_{fuel} = 20 mL, m_{cat} = 0.01 g, 100 mL min^{-1} of O_2, T = 120 °C.	All compounds were completely removed within 6 h of reaction. DBT displayed much faster kinetics compared to 4-MDBT and 4,6-DMDBT. Upon adding other components of diesel in the simulated fuel (Cyclohexane, Paraxylene, and 1-Octene), the desulfurization rate decreased. However, it was still possible to achieve 100% removal, requiring longer reaction times. >98% maintained for 7 cycles.	[155]
DBT, BT, or 4,6-DMDBT in n-Octane ($[S]_0$ = 500 µg mL^{-1})	V_2O_5@C	CHP	N.M.	V_{fuel} = 10 mL, m_{cat} = 50 mg, V_{CHP} = 0.17 mL, T = 60 °C, t = 5 h.	BT has the lowest desulfurization (63%), followed by 4,6-DMDBT (80%) and DBT (100%). Up to 7 cycles with no obvious decrease in catalytic activity.	[156]
DBT in Tridecane (C_0 = 100–2000 µg g^{-1})	FePc (NO$_2$)$_3$-CF	O_2	N.M.	V_{fuel} = 25 mL, m_{cat} = 0.25 g, 0.2 MPa of O_2 initial pressure, T = 130 °C.	Upon increasing initial concentration, DBT conversion decreased from 100% to 60% (100 and 2000 Mg G^{-1} initial DBT concentration, respectively).	[118]
DBT, 4,6-DMDBT or BT in n-Octane ($[S]_0$ = 250–500 ppm)	[PSPy]$_3$PMo$_{12}$O$_4$/GC	H_2O_2	Oxidized Compounds were removed in the catalyst phase	V_{fuel} = 5 mL, m_{cat} = 0.05 g, V_{H2O2} = 24 µL (H_2O_2/S = 3), T = 50 °C.	Removals were 100%, 90% and 50% for DBT, 4,6-DMDBT and BT, respectively. Results were maintained for 6 cycles.	[128]
DBT, 4-MDBT or 4,6-DMDBT in n-Octane ($[S]_0$ = 500 ppm)	TiO$_2$/GC	H_2O_2	Oxidized products extracted in the catalyst phase.	V_{fuel} = 5 mL, m_{cat} = 0.01 g, V_{H2O2} = 32 µL (H_2O_2/S = 4), T = 50 °C.	With a 10% loading of Tio$_2$, the best desulfurization performance was observed (100% in 40 min maintained for 10 cycles). Desulfurization for 4,6-DMDBT and 4-MDBT were 77 and 99%, respectively. Upon adding 5-10 Wt.% of P-Xylene in the fuel, desulfurization was not greatly affected (100 and 96%, respectively). a slight decrease was observed by adding 5 or 10 Wt.% of cyclohexane (85 and 75%, respectively). The radical •O$_2^-$ was found as the main active constituent in the ODS of DBT.	[119]

Legend: 3D-g-C$_3$N$_4$ = three-dimensional graphitic carbon nitride. AC = activated carbon. CA = carbon aerogel. CF = carbon fibers. CHP = cumene hydroperoxide. CNT = carbon nanotube. GC = graphitic carbon. GNF = graphitized carbon nanofiber. GO = graphene oxide. MC = mesoporous carbon. P[C$_2$VP] Br = Poly (N-ethyl-4-vinylpyridinium bromide). PPDA = Poly diallyldimethylammonium chloride. [PSPy] = N-(3-sulfonate propyl)-pyridinium. TBHP = tert-butyl hydroperoxide.

Table 10. ODS with carbon hybrid materials in photocatalytic systems.

Fuel	Catalyst	Oxidant	Extractant	Operational Conditions	Main Results	Ref.
DBT ($[S]_0$ = 500 ppm), BT ($[S]_0$ = 250 ppm), and RSH ($[S]_0$ = 250 ppm) in Acetonitrile	TiO$_2$/g-C$_3$N$_4$	H$_2$O$_2$	1-Methyl-2-Pyrrolidone	V_{fuel} = 20 mL, m_{cat} = 0.2 g, H$_2$O$_2$/S = 7, T = 30 °C, t = 2 h, 250 W High-Pressure Hg Lamp. 2-Step Process.	S removal was higher in the photocatalytic system. RSH compounds were more easily removed (100%) compared to BT and DBT (90%).	[123]
DBT in n-Octane ($[S]_0$ = 200 ppm)	CeO$_2$/Attapulgite/g-C$_3$N$_4$	H$_2$O$_2$	ACN	Mass Ratio Cat/DBT = 1:10, Molar Ratio H$_2$O$_2$/DBT = 1:4, t = 3 h, 300 W Xenon Lamp. 2-Step Process	A 100% removal of DBT. Conversion maintained above 90% for up to 8 cycles.	[124]
DBT in n-octane ($[S]_0$ = 200 ppm)	CQD/Attapulgite	H$_2$O$_2$	ACN	Mass Ratio Cat/Fuel = 1:1000, t = 5 h, 300 W Xenon Lamp. 2-Step Process	A 92.3% removal of DBT.	[125]
Th in n-Octane (C_0 = 800 μL L−1)	ZnTcPc/g-C$_3$N$_4$	O$_2$	CH$_2$Cl$_2$	V_{fuel} = 100 mL, m_{cat} = 20 mg, Visible Light Irradiation. 2-Step Process.	A 85% removal of DBT in 90 min.	[126]
DBT or 4,6-DMDBT in Tetradecane ($[S]_0$ = 200 ppm)	CNT/TiO$_2$	NA	Adsorption with Silica.	V_{fuel} = 100 mL, m_{cat} = 1 g, High-Pressure Hg Lamp.	Desulfurization in simulated Matrix: 80% for DBT and 70% for 4,6-DMDBT.	[127]
Commercial Diesel ($[S]_0$ = 714 ppm)	CNT/TiO$_2$	NA	Adsorption with Silica.	V_{fuel} = 100 mL, m_{cat} = 1 g, High-Pressure Hg Lamp.	S content decreased to 0 ppm after 120 min of reaction.	[127]

Legend: ACN = acetonitrile. CNT = carbon nanotube. g-C$_3$N$_4$ = graphitic carbon nitride. NA = not applicable.

Table 11. ODS with carbon-based materials as catalysts on their own.

Fuel	Catalyst	Oxidant	Extractant	Operational Conditions	Main Results	Ref.
DBT in n-Octane ([S]$_0$ = 500 ppm)	oCNT	H$_2$O$_2$	IL: OmimPF$_6$	V$_{fuel}$ = 5 mL, V$_{IL}$ = 1 mL, m$_{cat}$ = 5 mg, V$_{H2O2}$ = 64 μL, T = 70 °C, t = 60 min.	Conversion of >95.8% for 5 cycles. Removals of 93.7 (4,6-DMDBT), 100 (DBT), 97.3 (2-MBT), 100 (3-MBT) and 100% (BT) were observed.	[134]
BT, DBT, or 4,6-DMDBT in n-Dodecane ([S]$_0$ = 427 ppm)	CNT	O$_2$	N.M.	m$_{fuel}$ = 30 g, m$_{cat}$ = 0.01 g, 150 mL min^{-1} of O$_2$, T = 150 °C, t = 40 min.	A 100% removal of DBT in less than 30 min. One hundred percent conversion was also obtained for BT (70 Min) and 4,6-DMDBT (45 min). A slight decrease was observed for 5 reuse cycles.	[136]
DBT in Dodecane ([S]$_0$ = 200 ppm)	N, O-doped GO	Air (O$_2$)	CCl$_4$	V$_{fuel}$ = 20 mL, m$_{cat}$ = 10 mg, 100 mL min^{-1} air flow, T = 120 °C. 2-step process.	Removals of 99.8 (DBT), 97.5 (4,6-DMDBT) and 88.7% (4-MDBT) in 8 h of reaction were observed.	[131]
Diesel Sample ([S]$_0$ = 400 ppm)	N, O-doped GO	Air (O$_2$)	CCl$_4$	V$_{fuel}$ = 20 mL, m$_{cat}$ = 10 mg, 100 mL min^{-1} Air Flow, T = 120 °C. 2-Step Process.	A 84% removal of sulfur was observed.	[131]
BT, DBT or 4,6-DMDBT in n-Decane ([S]$_0$ = 500–1100 ppm)	GO	Air (O$_2$)	ACN	V$_{fuel}$ = 15 mL, V$_{ACN}$ = 7.5 mL, m$_{cat}$ = 0.6 mg, 20 mL min^{-1} air flow, 4.5 mL formic acid, T = 25 °C, t = 140 min, Mercury Lamp (100 W, peak at 365 nm).	A removal of >99.5% of sulfur was observed. High removal rates were maintained for 3 cycles.	[137]
DBT, BT, 3-MBT and 4,6-DMDBT in Dodecane ([S]$_0$ = 400 ppm)	rGO	O$_2$	N.M.	V$_{fuel}$ = 25 mL, m$_{cat}$ = 5 mg, 200 mL min^{-1} O$_2$ flow, T = 140 °C, t = 6 h.	Removals of 96.1 (3-MBT), 90.5 (BT), 100 (DBT), and 97.7% (4,6-DMDBT) observed.	[135]
Jet fuel (JP-8) ([S]$_0$ = 717 ppm)	AC	H$_2$O$_2$ + formic acid	N.M.	V$_{fuel}$ = 10 mL, m$_{cat}$ = 0.1 g, V$_{oxidant}$ = 2 mL, T = 25 °C, t = 4 h.	Acid treatment leads to better removal performance compared to ammonia treatment. Removals in the range of 41–69% were obtained.	[138]
JP-8 ([S]$_0$ = 717 ppm)	AC	H$_2$O$_2$ + formic acid	Adsorption with alumina	V$_{fuel}$ = 36 mL, m$_{cat}$ = 0.3 g, V$_{oxidant}$ = 7 mL, T = 60 °C, t = 60 min, Ultrasound: 20 kHz, and Amplitude of 60%.	Over 94% of sulfur was removed.	[132]
Ultra-Low-Sulfur Diesel (ULSD) ([S]$_0$ = 9 ppmw)	AC	H$_2$O$_2$ + formic acid	Adsorption with alumina	V$_{fuel}$ = 36 mL, m$_{cat}$ = 0.3 g, V$_{oxidant}$ = 7 mL, T = 60 °C, t = 60 min, Ultrasound: 20 kHz, and amplitude of 60%.	It was possible to obtain a fuel with less than 1 ppm of sulfur.	[132]
Commercial Diesel ([S]$_0$ = 2189 ppm)	AC	H$_2$O$_2$	ACN	V$_{fuel}$ = 50 mL, m$_{cat}$ = 0.5 g, H$_2$O$_2$/S = 3, Acetic Acid, 0.5 g of Tetraproprylammonium Bromide, T = 50 °C, t = 1 h.	For single oxidation, 60% removal of sulfur was observed. After 3 consecutive oxidations, 88–92% removal was observed.	[133]
4,6-DMDBT in Hexadecane (C_0 = 200 ppm)	AC	H$_2$O$_2$	Adsorption on the catalyst.	V$_{fuel}$ = 10 mL, m$_{cat}$ = 25 mg, V$_{H2O2}$ = 1 mL, T = 60 °C, t = 24 h.	A 75% removal of 4,6-DMDBT for original AC. After oxidation of AC, 100% removal was observed in only 10 min.	[130]
JP-8 fuel ([S]$_0$ = 1400 or 720 ppm)	AC	H$_2$O$_2$	Adsorption with alumina.	V$_{fuel}$ = 180 mL, V$_{H2O2}$ = 35 mL, 10 mL of formic acid, m$_{cat}$ = 120 mg, T = 60 °C, t = 90 min.	Oxidation only resulted in a small sulfur removal (3–20%). Combining with adsorption, results improved (75–95%).	[157]

Legend: N.M. = not mentioned. AC = activated carbon. ACN = acetonitrile. CNT = carbon nanotube. GO = graphene oxide. IL = ionic liquid. oCNT = oxidized carbon nanotube. rGO = reduced GO.

Table 12. ODS using H_2O_2 with amphiphilic carbon-based materials as catalysts.

Fuel	Catalyst	Extractant	Operational Conditions	Main Results	Ref.
DBT in n-dodecane (C_0 = 100–1000 ppm)	GO/COOH	Adsorption	V_{fuel} = 25 mL, m_{cat} = 0.05 g, V_{H2O2} = 5 mL, T = 273–313 K, 20 kHz Ultrasound Apparatus at 120 W	A 95% removal of sulfur was achieved for an initial concentration of DBT of 1000 ppm.	[139]
DBT, BT or 4,6-DMDBT in n-Octane ($[S]_0$ = 500 ppm)	$PW_{12}O_{40}-$/C-Si	ACN	V_{fuel} = 1 mL, V_{ACN} = 1 mL, 4 wt.% of Catalyst, H_2O_2/S = 6, T = 60 °C, 5 min in US to form an emulsion, t = 1 h.	Maximum conversion of 99.86% maintained for 5 cycles.	[147]
Two Real Oil Samples ($[S]_0$ = 968.72 and 2668.78 ppm)	$PW_{12}O_{40}-$/C-Si	ACN	V_{fuel} = 1 mL, V_{ACN} = 1 mL, 4 wt.% of catalyst, H_2O_2/S = 6, T = 60 °C, 5 min in US to form an emulsion, t = 1 h.	Three consecutive cycles of ODS resulted in s content lower than 10 ppm.	[147]
DBT in Cyclohexane ($[S]_0$ = 50 ppm)	Fe/C and FeMo/C	Aqueous H_2O_2 Phase	V_{fuel} = 5 mL, m_{cat} = 15 mg, V_{H2O2} = 1 mL, T = 25 °C, t = 120 min. Emulsion	>60% conversion of DBT for up to 3 cycles.	[143]
DBT in n-Octane ($[S]_0$ = 250 ppm)	SiO_2@C-dots/$[PW_{12}O_{38}]^{3-}$	ACN	V_{fuel} = 60 mL, V_{ACN} = 60 mL, m_{cat} = 0.2 g, Molar Ratio H_2O_2/DBT = 3, T = 60 °C, t = 3 h.	100% removal of DBT in 180 min.	[158]
DBT in Cyclohexane ($[S]_0$ = 50 ppm)	Si-C	Aqueous H_2O_2 Phase	V_{fuel} = 5 mL, m_{cat} = 10 mg, V_{H2O2} = 1 mL, t = 180 min. Emulsion	Maximum removal of 15 mgs g_{cat}^{-1} observed	[144]
Diesel S1800 ($[S]_0$ = 1800 ppm)	Si-C	Aqueous H_2O_2 Phase	V_{fuel} = 5 mL, m_{cat} = 10 mg, V_{H2O2} = 1 mL, t = 180 min. Emulsion	A 57% removal of sulfur in Diesel S1800.	[144]
DBT in n-Octane (C_0 = 800 ppm)	$H_3PMo_{12}O_{40}$/AmHMSiO$_2$@C	ACN	V_{fuel} = 2 mL, V_{ACN} = 2 mL, n_{cat} = 0.002 mmol, n_{H2O2} = 0.15 mmol, T = 40 °C, t = 3 h.	>99% conversion was obtained in 180 min and maintained for 5 cycles.	[140]
DBT (C_0 = 500 ppm), 4-MDBT (C_0 = 200 pm), 4,6-DMDBT (C_0 = 200 ppm) in Dodecane	g-C_3N_4	Adsorption	V_{fuel} = 5 mL, m_{cat} = 0.05 g, H_2O_2/S = 4, T = 60 °C, t = 60 min, 800 rpm.	A 100% removal of DBT and ~80% for 4-MDBT and 4.6-DMDBT.	[141]
Th and DBT in Cyclohexane (C_0 = 100 ppm)	CNT/red mud	Aqueous H_2O_2 Phase	V_{fuel} = 5 mL, m_{cat} = 20 mg, V_{H2O2} = 1 mL, Emulsion	67% removal of Th and 82% of DBT in 1 h.	[145]
DBT in Cyclohexane (C_0 = 500 ppm)	FeMo/CNT	Aqueous H_2O_2 Phase	V_{fuel} = 5 mL, m_{cat} = 20 mg, V_{H2O2} = 1 mL, Emulsion	Oxidation Efficiency Varied Between 20–100%.	[146]

Table 12. *Cont.*

Fuel	Catalyst	Extractant	Operational Conditions	Main Results	Ref.
DBT in n-dodecane (C_0 = 100–1000 ppm)	GO/COOH	Adsorption	V_{fuel} = 25 mL, m_{cat} = 0.05 g, V_{H2O2} = 5 mL, T = 273–313 K, 20 kHz Ultrasound Apparatus at 120 W	A 95% removal of sulfur was achieved for an initial concentration of DBT of 1000 ppm.	[139]
DBT in n-Heptane (C_0 = 0.1 wt.%)	[Bmin]$_3$PMo$_{12}$O$_{40}$/g-C$_3$N$_4$	Aqueous H$_2$O$_2$ Phase	V_{fuel} = 25 mL, m_{cat} = 0.05 g, H$_2$O$_2$/S = 3, T = 40 °C, t = 120 min, 250 W Sodium Lamp.	The DBT conversion increased from ~30% to 94.5% in 120 min of reaction with visible light. The active species in DBT oxidation was found to be HO•.	[142]
DBT in toluene (C_0 = 50 ppm)	Fe$_2$O$_3$/C	MeOH	V_{fuel} = 9.9 mL, m_{cat} = 10 mg, $V_{oxidant}$ = 0.1 mL (H$_2$O$_2$/HCOOH (1:1 mol/mol)), T = 25 °C. 2-Step Process.	A 97% Conversion of DBT in 180 min of reaction, with a yield towards sulfones of ~60%. In the presence of QN, the yield towards the sulfone decreased to below 40%.	[159]
DBT in cyclohexane ([S]$_0$ = 50 ppm)	Au/RmEtb	Aqueous H$_2$O$_2$ Phase	V_{fuel} = 5 mL, m_{cat} = 20 mg, V_{H2O2} = 1 mL.	The highest removal rate of DBT was attained with the catalyst containing a carbon coating due to the amphiphilic characteristics (removal of ~4.5 mg$_S$ g$_{cat}^{-1}$)	[160]
Th, BT and DBT in n-Heptane ([S]$_0$ = 500 ppm)	C$_3$N$_2$H$_5$@H$_3$PMo$_{12}$O$_{40}$@CS	ACN	V_{fuel} = 50 mL, m_{cat} = 0.1 g, $V_{oxidant}$ = 3 mL (H$_2$O$_2$/acetic acid), T = 30–35 °C, t = 1 h. 2-step process	>96% removal of S was possible depending on the condition applied.	[161]
Real Gasoline ([S]$_0$ = 0.498 wt.%)	C$_3$N$_2$H$_5$@H$_3$PMo$_{12}$O$_{40}$@CS	ACN	V_{fuel} = 50 mL, m_{cat} = 0.1 g, $V_{oxidant}$ = 3 mL (H$_2$O$_2$/acetic acid), T = 30–35 °C, t = 1 h. 2-step process	Over 95% removal of S was observed while not impacting other parameters (density, salt content, water content, and distillation point).	[161]

Legend: ACN = acetonitrile. AmHMSiO$_2$ = amphiphilic hollow mesoporous silica. C-dots = carbon dots. CNT = carbon nanotube. g-C$_3$N$_4$ = graphitic carbon nitride. GO = graphene oxide. MeOH = methanol. RmEt = red mud residue modified by chemical vapor deposition using ethanol as carbon source.

4. Carbon Materials in ODN

Denitrogenation reactions are not as widely studied as desulfurization, and thus there is a limited number of papers regarding denitrogenation with carbon-based materials. In general, the roles of the carbon-based materials in ODS are similar in ODN reactions. Many authors highlighted the amphiphilicity of carbon structures as beneficial in ODN reactions. Table 13 summarizes the papers related to ODN reactions. As observed, most of the works deal with ODN of QN (model component most extensively studied). ODN is mainly conducted with H_2O_2 using iron-containing carbon materials under mild conditions (25–80 °C) for reaction times up to 3 h (achieving complete oxidation of the model molecule at lower times depending on the selected catalyst and operating conditions). The selection of iron catalyst with H_2O_2 as oxidant may be ascribed to the reactive iron- H_2O_2 pair, also known as Fenton-reagent [162,163].

Guimarães et al. (2013) have tested magnetite covered by carbon as the catalyst for the simultaneous oxidation of DBT and QN in a biphasic system (toluene-acetonitrile, $[QN]_0$ = 50 ppm) [159]. DBT conversion was higher than QN conversion (100% instead of ~60% for QN). The presence of DBT reduced QN oxidation by about 50%. The authors have highlighted the amphiphilicity of the catalyst and its ability to remain in the interface between the two solvents as one of the critical conditions to display high catalytic activity [159].

Mambrini et al. (2017) studied the removal of QN in cyclohexane ($[N]_0$ = 50 ppm) [143] in a PIC-like system using a FeMo/C as the catalyst. Due to the amphiphilic character of the catalyst, it can interact with aqueous and oily phases, stabilizing an emulsion cyclohexane-aqueous H_2O_2. The emulsified system increases the interfacial area and enhances the reaction rate. The high interfacial area resulted in a very fast conversion of QN: almost complete conversion in less than 10 min [143]. FeMo/C revealed a higher catalytic activity than Fe/C, which was ascribed to the higher content of carbon on FeMo/C. Higher carbon content allowed a better interaction between the oily and the aqueous phase, favoring emulsion stabilization [143].

Oliveira et al. (2014) prepared amphiphilic catalysts through the modification of red mud by chemical vapor deposition (CVD) of ethanol [145]. The materials were tested in the PIC-like oxidation of QN in cyclohexane with H_2O_2. Within 60 min, QN was removed entirely, and this activity was maintained for 5 cycles. They ascribed the exciting results to the amphiphilicity resulting from the carbon deposits after CVD, which allowed the stabilization of the emulsified system, increasing the contact between the organic and the aqueous phases [145]. Similar materials were synthesized by Teixeira et al. (2013) [146] and applied in the biphasic oxidation of QN in a PIC-like system. One hundred percent oxidation of QN was possible in less than 30 min of reaction. The efficiency of the reaction system was maintained for 5 cycles [146].

Souza, Pereira, and Oliveira (2012) produced amphiphilic catalysts based on onion-like carbon (OLC) over iron oxide and applied them in the biphasic oxidation of QN in toluene [164]. Ninety three percent removal of QN was obtained. The activity of the material was ascribed to increased contact between the aqueous oily phases due to the presence of a hydrophobic carbon layer on the catalyst [164].

Oliveira et al. (2020) prepared N-doped CNTs over red mud and applied them in the biphasic oxidation of QN in cyclohexane ($[N]_0$ of 30 ppm) with H_2O_2 [165]. The catalysts were synthesized sequentially feeding ethylene (as carbon source) and acetonitrile (as carbon and nitrogen sources), leading to 4 different samples. (i) A completely undoped (synthesized using only ethylene); (ii) a completely N-doped (synthesized using only acetonitrile); and (iii) two samples synthesized using both precursors during different times, leading to two partially N-doped samples. QN oxidation varied according to the content of nitrogenated groups on the material: higher N contents led to increased removal of QN (80% versus 44%) [165]. A study with similar materials was previously done by Purceno et al. (2015) [166]. However, the selectively N-doped CNTs acted only as emulsion stabilizers in their case, and a homogeneous catalyst (Fe^{+2}) was applied. Without the

presence of the CNTs, only 10% of QN was removed. On the other hand, by adding amphiphilic CNTs, a removal of QN in the range 85–100% was observed in 15–40 min of reaction, depending on the CNT sample. The results were directly ascribed to the ability of amphiphilic CNTs to stabilize Pickering emulsions, increasing interfacial area [166].

Ammar, Kareem, and Mohammed (2020) studied exclusively the ultrasound-assisted catalytic oxidative-adsorptive denitrogenation (COADN) of pyrrole (PYR) and indole (IND) (dissolved in n-nonane, $[PYR]_0$ and $[IND]_0$ of 200 ppm) [167] using a PMo-Fe_2O_3/rGO as the catalyst. Upon increasing sonication power and time, oxidation of N compounds increased. The best results were obtained with 200 W ultrasound power for 240 min, leading to 86 and 90% conversion for PYR and IND, respectively. Compared to the silent reaction (no ultrasound), an increase in 50 and 58% removals for PYR and IND, respectively, were observed. This high conversion was maintained for up to 5 cycles [167]. The authors did not highlight the role of the carbon structure.

Raffie and Khodayari (2017) added N compounds to a simulated fuel containing DBT in order to investigate the influence of the presence of N compounds (IND, QN, pyridine, and pyrrole, C_0 = 60 ppm) in the removal of DBT using a catalyst containing PMoV/Fe_3O_4/g-C_3N_4 [76]. All nitrogenated compounds were oxidized in very short reaction times (20 min). Although the presence of N compounds slowed DBT oxidation, the effect was minimal. Thus, proving that desulfurization and denitrogenation can be conducted simultaneously for the proposed system [76]. A similar study was performed previously by the same group [84] using an HPW/TiO_2/GC catalyst. They have also concluded that the addition of nitrogenated compounds slightly impacts DBT removal. However, they have not reported the conversion of those nitrogenated compounds in the system.

Bhadra et al. (2019) studied the denitrogenation of a simulated fuel containing a range of different N compounds (IND, 1-, 2- and 3-methyl-substituted indoles (1-Me-IND, 2-Me-IND, and 3-Me-IND, respectively), PYR, carbazole (CBZ), and QN in n-octane, C_0 = 5000 ppm) [168]. The biphasic oxidation was conducted in the presence of acetic acid and with H_2O_2 as the oxidant. For IND, upon increasing the H_2O_2/N ratio and catalyst dosage up to a certain point (H_2O_2/N = 10 and catalyst concentration of 0.25 g L^{-1}), IND removal increased. However, further increasing any of those parameters did not have a significant impact on IND removal. The removal of the remaining N compounds was also investigated. In 120 min of reaction, ~90% of IND was removed (maintained for 4 cycles), followed closely by 2-Me-IND. Removals of 1-Me-IND and 3-Me-IND were ~70%, whereas PYR and CBZ removals were 40% and <20%, respectively. QN was not oxidized in the studied conditions. The distinction between the oxidation rate of different compounds was ascribed to the electron density around the N atom, similar to that observed with S compounds. However, the authors have highlighted that further studies are necessary to truly understand the relation between electron density in N compounds and reaction rate [168]. The authors did not highlight the role of the carbon structure.

Table 13. ODN reactions using carbon-based materials and H_2O_2 as oxidant.

Fuel	Catalyst	Extractant	Operational Conditions	Main Results	Ref.
IND or PYR in n-Nonane (C_0 = 50–800 ppm)	$H_3PMo_{12}O_{40}$-Fe_3O_4/rGO	Aqueous H_2O_2 phase	V_{fuel} = 50 mL, C_{cat} = 0–2 g L^{-1}, Molar Ratio H_2O_2/PYR = 0–10, t = 15–240 min, US: 50–300 W.	Increasing ultrasound (US) power (to 200 W) increases denitrogenation (max. 90% in 240 min). Increasing the H_2O_2/PYR molar ratio over 5 did not increase n removal. Five cycles of reuse were possible.	[167]
QN in Toluene (C_0 = 100 ppm in the presence of 50 ppm of DBT)	Fe_2O_3/C	Aqueous H_2O_2 phase	V_{fuel} = 9.9 mL, m_{cat} = 10 mg, $V_{oxidant}$ = 0.1 mL (H_2O_2/HCOOH), T = 25 °C, pH 4 (natural pH).	Approximately 60% removal of QN. The presence of DBT inhibited the complete removal of QN.	[159]
QN in Cyclohexane ($[N]_0$ = 50 ppm)	Fe/C and FeMo/C	Aqueous H_2O_2 phase	V_{fuel} = 5 mL, m_{cat} = 15 mg, V_{H2O2} = 1 mL, T = 25 °C, natural pH.	100% removal of QN in 120 min of reaction.	[143]
QN in Cyclohexane ($[N]_0$ = 30 ppm)	N-Doped CNT/Red Mud	Aqueous H_2O_2 phase	V_{fuel} = 5 mL, m_{cat} = 20 mg, V_{H2O2} = 1 mL.	Maximum removal of 80% in 45 min of reaction.	[165]
DBT + IND, Quinolone, PYR, Pyrrole in EtOH: Hexane (1:1 vol. ratio) (C_0 = 60 ppm in the presence of 1000 ppm of DBT)	$H_5PMo_{10}V_2O_{40}$/Fe_3O_4/g-C_3N_4	EtOH	V_{fuel} = 5 mL, m_{cat} = 0.03 g, n_{H2O2} = 10 mmol, T = 80 °C.	All N-containing compounds were wholly oxidized in 20 min of reaction. Their presence did not affect to a great extent the removal of DBT.	[76]
QN in Cyclohexane (C_0 = 500 ppm)	WEEE Impregnated in Clay and Hydrophobized with CTAB.	ACN	V_{fuel} = 10 mL, V_{ACN} = 2 mL, V_{H2O2} = 320 µL, T = 60 °C, t = 3 h.	A maximum removal rate of 73.5 mg_{QN} g_{cat}^{-1}	[169]
IND, 1Me-IND, 2Me-IND, 3Me-IND, PYR, QN, or CBZ in n-Octane (C_0 = 5000 ppm)	TiO_2@porous C	Acetic Acid	V_{fuel} = 20 mL, $V_{extractant}$ = 2 mL, C_{cat} = 0–0.5 g L^{-1}, H_2O_2/N = 0–15, T = 30–50 °C, t = 5–120 min, 100–1000 rpm, 5–10 wt.% water.	Increasing O/N up to 10 and catalyst dosage up to 0.25 g L^{-1} results in an increase in N removal. Further increasing those values does not alter the results. Denitrogenation varied between 15–90%, depending on the N compound. Similar results were maintained for 4 cycles.	[168]
QN in Cyclohexane (C_0 = 500 ppm)	C/red mud	Aqueous H_2O_2 Phase	V_{fuel} = 5 mL, m_{cat} = 20 mg, V_{H2O2} = 1 mL.	100% removal of QN in 60 min of reaction.	[145]
QN in Cyclohexane (C_0 = 500 ppm)	$FeCl_2 \cdot 4H_2O$	Aqueous H_2O_2 Phase	V_{fuel} = 5 mL, C_{cat} = 5.6 mmol L^{-1} and 1 wt.% CNT, V_{H2O2} = 300 µL, 300 µL of formic acid, 20 s sonication to form an emulsion.	Depending on the Sample (i.e., whether it is amphiphilic), 100% removal of QN is observed in 15 min.	[166]
QN in Toluene (C_0 = 25 ppm)	Fe/OLC	Aqueous H_2O_2 Phase	V_{fuel} = 10 mL, m_{cat} = 10 mg, C_{H2O2} = 0.05 mol L^{-1}, T = 25 °C, pH 6.	Maximum removal observed was 93%	[164]
QN in Cyclohexane ($[N]_0$ = 500 ppm)	FeMo/CNT	Aqueous H_2O_2 Phase	V_{fuel} = 5 mL, m_{cat} = 20 mg, V_{H2O2} = 1 mL.	100% QN oxidation in 30 min of reaction.	[146]

Legend: ACN = acetonitrile. CNT = carbon nanotube. CTAB = cetyltrimethylammonium bromide. EtOH = ethanol. g-C_3N_4 = graphitic carbon nitride. OLC = onion like carbon. rGO = reduced graphene oxide. WEEE = waste electrical and electronic equipment.

5. Final Considerations and Perspectives

Carbon-based materials have proved to be interesting materials that can be used in ODS and ODN processes under different systems. The facility to tune their properties and combine with other materials to form hybrid materials makes them attractive when designing effective catalysts for desulfurization and denitrogenation. Especially in biphasic systems, their developed surface areas, which impact the dispersion of active phases and an increased adsorption capacity towards S pollutants, have been pointed out as a key contribution of those materials, mainly for hybrid catalysts. Besides that, carbon materials were found to benefit ultrasonic cavitation, boosting reaction in ultrasound-assisted processes. Their usual hydrophobic nature increases the interaction with fuels and lipophilic pollutants, such as sulfur compounds, allowing them to act as phase transfer agents to extract these S compounds. Finally, they were found to accelerate electron mobility, and in photocatalytic systems, they avoid electron-hole recombination. When considering carbon-based materials as catalysts on their own, their activity is mainly ascribed to the presence of oxygenated groups and defect sites. However, there is still some controversy on how each influences the desulfurization capacity. In amphiphilic materials, carbon-based materials were again used as catalysts on their own and in hybrid forms. Their main contribution comes from stabilizing PIC-like systems, where the material acts simultaneously as a catalyst and as an emulsifier.

However, a few points must be raised. (i) There are much more reports related to the application of carbon-based hybrid materials and much less related to carbonaceous structures as catalysts on their own. However, the results reported in this review point out that carbon materials have allowed similar removals to those observed with hybrid materials. Thus, there is still the opportunity to study carbon-based materials as catalysts on their own for desulfurization and denitrogenation. (ii) There is also a lack of reports testing carbon-based materials as catalysts on their own containing dopants other than oxygen. Nitrogen, phosphorus, and sulfur are all possible dopants that have been shown to increase catalytic activity in aqueous phase oxidation reactions [64,170–172]. (iii) Denitrogenation approaches are much less common, and there is still the opportunity to study denitrogenation reactions, mainly aiming at simultaneous high removals of N and S-containing compounds. (iv) There are very few works dealing with the use of catalysts prepared from renewable or waste sources. Environmental aspects related to the catalyst (metal leaching species and waste generation, among others), economic issues, or life cycle assessment (LCA) are not reported by any papers. (v) Most authors fail to explain the role of the carbonaceous structure in the process, or the advantages of using carbon-based materials, mainly when considering carbon-based composites for ODS and ODN purposes. Understanding the role of each component of the catalyst is critical to developing outstanding catalysts.

References

1. Eurostat. Available online: https://ec.europa.eu/eurostat/databrowser/view/nrg_bal_c/default/table?lang=en (accessed on 13 July 2021).
2. Walters, C. Petroleum. In *Kirk-Othmer Encyclopedia of Chemical Technology*; John Wiley & Sons, Inc.: Hoboken, NJ, USA, 2020; pp. 1–44. [CrossRef]
3. Marafi, A.; Albazzaz, H.; Rana, M.S. Hydroprocessing of heavy residual oil: Opportunities and challenges. *Catal.Today* **2019**, *329*, 125–134. [CrossRef]
4. Prado, G.H.C.; Rao, Y.; de Klerk, A. Nitrogen Removal from Oil: A Review. *Energy Fuels* **2017**, *31*, 14–36. [CrossRef]
5. Sikarwar, P.; Gosu, V.; Subbaramaiah, V. An overview of conventional and alternative technologies for the production of ultra-low-sulfur fuels. *Rev. Chem. Eng.* **2019**, *35*, 669–705. [CrossRef]
6. Ball, J.S.; Whisman, M.L.; Wenger, W.J. Nitrogen Content of Crude Petroleum. *Ind. Eng. Chem.* **1951**, *43*, 2577–2581. [CrossRef]
7. Ahmad, W. Sulfur in Petroleum: Petroleum Desulfurization Techniques. In *Applying Nanotechnology to the Desulfurization Process in Petroleum Engineering*; Saleh, T.A., Ed.; Engineering Science Reference: Hershey, PA, USA, 2016; pp. 1–50.
8. Song, C.; Ma, X. New design approaches to ultra-clean diesel fuels by deep desulfurization and deep dearomatization. *Appl. Catal. B* **2003**, *41*, 207–238. [CrossRef]
9. Romanow-Garcia, S.; Hoffman, H.L. Petroleum and Its Products. In *Riegel's Handbook of Industrial Chemistry*, 10th ed.; Kent, J.A., Ed.; Kluwer Academic/Plenum Publishers: New York, NY, USA, 2003; pp. 506–544.
10. Lloyd, A.C.; Cackette, T.A. Diesel engines: Environmental impact and control. *J. Air Waste Manag. Assoc.* **2001**, *51*, 809–847. [CrossRef]
11. Kampa, M.; Castanas, E. Human health effects of air pollution. *Environ. Pollut.* **2008**, *151*, 362–367. [CrossRef] [PubMed]
12. Pénard-Morand, C.; Annesi-Maesano, I. Air pollution: From sources of emissions to health effects. *Breathe* **2004**, *1*, 108–119. [CrossRef]
13. Cohen, A.J.; Pope III, C.A. Lung Cancer and Air Pollution. *Environ. Health Perspect.* **1995**, *103*, 219–224.
14. Sunyer, J. The association of daily sulfur dioxide air pollution levels with hospital admissions for cardiovascular diseases in Europe (The Aphea-II study). *Eur. Heart J.* **2003**, *24*, 752–760. [CrossRef]
15. Wu, Y.; Li, R.; Cui, L.; Meng, Y.; Cheng, H.; Fu, H. The high-resolution estimation of sulfur dioxide (SO_2) concentration, health effect and monetary costs in Beijing. *Chemosphere* **2020**, *241*, 125031. [CrossRef]
16. Grennfelt, P.; Engleryd, A.; Forsius, M.; Hov, O.; Rodhe, H.; Cowling, E. Acid rain and air pollution: 50 years of progress in environmental science and policy. *Ambio* **2020**, *49*, 849–864. [CrossRef] [PubMed]
17. Burns, D.A.; Aherne, J.; Gay, D.A.; Lehmann, C.M.B. Acid rain and its environmental effects: Recent scientific advances. *Atmos. Environ.* **2016**, *146*, 1–4. [CrossRef]
18. Gandhi, H.S.; Shelef, M. Effects of sulphur on noble metal automotive catalysts. *Appl. Catal.* **1991**, *77*, 175–187. [CrossRef]
19. Council of the European Union. Official Journal of the European Union 140, Directive 2009/30/EC of the European Parliament and of the Council of 23 April 2009 Amending Directive 98/70/EC as Regards the Specification of Petrol, Diesel and Gas-Oil and Introducing a Mechanism to Monitor and Reduce Greenhouse Gas Emissions and Amending Council Directive 1999/32/EC as Regards the Specification of Fuel Used by Inland Waterway Vessels and Repealing Directive 93/12/EEC. 2009. Available online: https://eur-lex.europa.eu/legal-content/EN/TXT/?uri=celex%3A32009L0030 (accessed on 23 April 2021).
20. Control of Air Pollution from Motor Vehicles: Tier 3 Motor Vehicle Emission and Fuel Standards (Final Rule). Environmental Protection Agency. Federal Register Vol. 79, n° 81, Monday, April 28th, 2014. Available online: https://www.govinfo.gov/content/pkg/FR-2014-04-28/pdf/2014-06954.pdf (accessed on 23 April 2021).
21. EPA-420-B-16-005-Highway and Nonroad, Locomotive, and Marine (NRLM) Diesel Fuel Sulfur Standards. Office of Transportation and Air Quality, 2016. Available online: https://nepis.epa.gov/Exe/ZyPDF.cgi?Dockey=P100O9ZH.pdf (accessed on 24 April 2021).
22. Miller, J.D.; Façanha, C. The State of Clean Transport Policy: A 2014 Synthesis of Vehicle and Fuel Policy Developments. International Council on Clean Transportation. Washington: International Council on Clean Transportation, 2014. Available online: https://theicct.org/publications/state-clean-transport-policy-2014-synthesis-vehicle-and-fuel-policy-developments (accessed on 10 June 2021).
23. Japan: Fuels: Diesel and Gasoline. Available online: https://www.transportpolicy.net/standard/japan-fuels-diesel-and-gasoline/ (accessed on 24 April 2021).
24. China: Fuels: Diesel and Gasoline. Available online: https://www.transportpolicy.net/standard/china-fuels-diesel-and-gasoline/ (accessed on 24 April 2021).
25. India: Fuels: Diesel and Gasoline. Available online: https://www.transportpolicy.net/standard/india-fuels-diesel-and-gasoline/ (accessed on 24 April 2021).
26. Russia: Fuels: Diesel and Gasoline. Available online: https://www.transportpolicy.net/standard/russia-fuels-diesel-and-gasoline-2/ (accessed on 24 April 2021).
27. Fuel Quality Standards (Petrol) Determination 2019, Minister for the Environment. 2019. Available online: https://www.legislation.gov.au/Details/F2019L00455 (accessed on 24 April 2021).

28. Regulation (EC) Nº. 715/2007 of the European Parliament and of the Council of 20 June 2007 on Type Approval of Motor Vehicles with Respect to Emissions from Light Passenger and Commercial Vehicles (Euro 5 and Euro 6) and on Access to Vehicle Repair and Maintenance Information. Available online: https://eur-lex.europa.eu/legal-content/EN/ALL/?uri=celex%3A32007R0715 (accessed on 24 April 2021).

29. Miller, J.; Jin, L. Global Progress Toward Soot-Free Diesel Vehicles in 2019. International Council on Clean Transportation, 2019. Available online: https://theicct.org/publications/global-progress-toward-soot-free-diesel-vehicles-2019 (accessed on 17 May 2021).

30. Fahim, M.A.; Alsahhaf, T.A.; Elkilani, A. Hydroconversion. In *Fundamentals of Petroleum Refining*; Fahim, M.A., Alsahhaf, T.A., Elkilani, A., Eds.; Elsevier: Oxford, UK, 2010; pp. 153–198.

31. Speight, J.G. Hydrotreating and Desulfurization. In *The Refinery of the Future*; Gulf Professional Publishing: Burlington, MA, USA, 2011; pp. 237–273. [CrossRef]

32. Mochida, I.; Choi, K.-H. An Overview of Hydrodesulfurization and Hydrodenitrogenation. *J. Jpn. Petrol. Inst.* **2004**, *47*, 145–163. [CrossRef]

33. Bachrach, M.; Marks, T.J.; Notestein, J.M. Understanding the Hydrodenitrogenation of Heteroaromatics on a Molecular Level. *ACS Catal.* **2016**, *6*, 1455–1476. [CrossRef]

34. Rajendran, A.; Cui, T.-y.; Fan, H.-x.; Yang, Z.-f.; Feng, J.; Li, W.-y. A comprehensive review on oxidative desulfurization catalysts targeting clean energy and environment. *J. Mater. Chem. A* **2020**, *8*, 2246–2285. [CrossRef]

35. Brunet, S.; Mey, D.; Pérot, G.; Bouchy, C.; Diehl, F. On the hydrodesulfurization of FCC gasoline: A review. *Appl. Catal. A* **2005**, *278*, 143–172. [CrossRef]

36. Babich, I. Science and technology of novel processes for deep desulfurization of oil refinery streams: A review. *Fuel* **2003**, *82*, 607–631. [CrossRef]

37. Ibrahim, M.H.; Hayyan, M.; Hashim, M.A.; Hayyan, A. The role of ionic liquids in desulfurization of fuels: A review. *Renew. Sustain. Energy Rev.* **2017**, *76*, 1534–1549. [CrossRef]

38. Abro, R.; Abdeltawab, A.A.; Al-Deyab, S.S.; Yu, G.; Qazi, A.B.; Gao, S.; Chen, X. A review of extractive desulfurization of fuel oils using ionic liquids. *RSC Adv.* **2014**, *4*, 35302–35317. [CrossRef]

39. Majid, M.F.; Mohd Zaid, H.F.; Kait, C.F.; Jumbri, K.; Yuan, L.C.; Rajasuriyan, S. Futuristic advance and perspective of deep eutectic solvent for extractive desulfurization of fuel oil: A review. *J. Mol. Liq.* **2020**, *306*, 112870. [CrossRef]

40. Svinterikos, E.; Zuburtikudis, I.; Al-Marzouqi, M. Carbon Nanomaterials for the Adsorptive Desulfurization of Fuels. *J. Nanotechnol.* **2019**, *2019*, 2809867. [CrossRef]

41. Speight, J.G.; El-Gendy, N.S. Biocatalytic Desulfurization. In *Introduction to Petroleum Biotechnology*; Gulf Professional Publishing: Oxford, UK, 2018; pp. 165–227. [CrossRef]

42. Li, J.; Yang, Z.; Li, S.; Jin, Q.; Zhao, J. Review on oxidative desulfurization of fuel by supported heteropolyacid catalysts. *J. Ind. Eng. Chem.* **2020**, *82*, 1–16. [CrossRef]

43. Hossain, M.; Park, H.; Choi, H. A Comprehensive Review on Catalytic Oxidative Desulfurization of Liquid Fuel Oil. *Catalyst* **2019**, *9*, 229. [CrossRef]

44. Haghighi, M.; Gooneh-Farahani, S. Insights to the oxidative desulfurization process of fossil fuels over organic and inorganic heterogeneous catalysts: Advantages and issues. *Environ. Sci. Pollut. Res. Int.* **2020**, *27*, 39923–39945. [CrossRef] [PubMed]

45. Otsuki, S.; Nonaka, T.; Takashima, N.; Qian, W.; Ishihara, A.; Imai, T.; Kabe, T. Oxidative Desulfurization of Light Gas Oil and Vacuum Gas Oil by Oxidation and Solvent Extraction. *Energy Fuels* **2000**, *14*, 1232–1239. [CrossRef]

46. Ogunlaja, A.S.; Abdul-quadir, M.S.; Kleyi, P.E.; Ferg, E.E.; Watts, P.; Tshentu, Z.R. Towards oxidative denitrogenation of fuel oils: Vanadium oxide-catalysed oxidation of quinoline and adsorptive removal of quinoline-N-oxide using 2,6-pyridine-polybenzimidazole nanofibers. *Arab. J. Chem.* **2019**, *12*, 198–214. [CrossRef]

47. Nicolaescu, A.R.; Wiest, O.; Kamat, P.V. Mechanistic pathways of the hydroxyl radical reactions of quinoline. 1. Identification, distribution, and yields of hydroxylated products. *J. Phys. Chem. A* **2005**, *109*, 2822–2828. [CrossRef]

48. Weeranoppanant, N. Enabling tools for continuous-flow biphasic liquid–liquid reaction. *Reac. Chem. Eng.* **2019**, *4*, 235–243. [CrossRef]

49. Xue, N.; Zhang, G.; Zhang, X.; Yang, H. A reinforced Pickering emulsion for cascade reactions. *ChemComm* **2018**, *54*, 13014–13017. [CrossRef] [PubMed]

50. Pera-Titus, M.; Leclercq, L.; Clacens, J.M.; De Campo, F.; Nardello-Rataj, V. Pickering interfacial catalysis for biphasic systems: From emulsion design to green reactions. *Angew. Chem. Int. Ed.* **2015**, *54*, 2006–2021. [CrossRef] [PubMed]

51. Jiang, H.; Sheng, Y.; Ngai, T. Pickering emulsions: Versatility of colloidal particles and recent applications. *Curr. Opin. Colloid Interface Sci.* **2020**, *49*, 1–15. [CrossRef]

52. Sjoo, M.; Rayner, M.; Wahlgren, M. Particle-stabilized Emulsions. In *Engineering Aspects of Food Emulsification and Homogenization*; Rayner, M., Dejmek, P., Eds.; CRC Press: Boca Raton, FL, USA, 2015; pp. 101–122.

53. Chevalier, Y.; Bolzinger, M.-A. Emulsions stabilized with solid nanoparticles: Pickering emulsions. *Colloids Surf. A Physicochem. Eng. Asp.* **2013**, *439*, 23–34. [CrossRef]

54. Briggs, N.; Raman, A.K.Y.; Barrett, L.; Brown, C.; Li, B.; Leavitt, D.; Aichele, C.P.; Crossley, S. Stable pickering emulsions using multi-walled carbon nanotubes of varying wettability. *Colloids Surf. A Physicochem. Eng. Asp.* **2018**, *537*, 227–235. [CrossRef]

55. Briggs, N.M.; Weston, J.S.; Li, B.; Venkataramani, D.; Aichele, C.P.; Harwell, J.H.; Crossley, S.P. Multiwalled Carbon Nanotubes at the Interface of Pickering Emulsions. *Langmuir* **2015**, *31*, 13077–13084. [CrossRef]

56. Wang, Z.; Wang, Y. Tuning Amphiphilicity of Particles for Controllable Pickering Emulsion. *Materials* **2016**, *9*, 903. [CrossRef]

57. Bhadra, B.N.; Jhung, S.H. Oxidative desulfurization and denitrogenation of fuels using metal-organic framework-based/-derived catalysts. *Appl. Catal. B* **2019**, *259*, 118021. [CrossRef]

58. Ribeiro, R.S.; Silva, A.M.T.; Figueiredo, J.L.; Faria, J.L.; Gomes, H.T. The influence of structure and surface chemistry of carbon materials on the decomposition of hydrogen peroxide. *Carbon* **2013**, *62*, 97–108. [CrossRef]

59. Fang, G.; Gao, J.; Liu, C.; Dionysiou, D.D.; Wang, Y.; Zhou, D. Key role of persistent free radicals in hydrogen peroxide activation by biochar: Implications to organic contaminant degradation. *Environ. Sci. Technol.* **2014**, *48*, 1902–1910. [CrossRef]

60. Vega, E.; Valdés, H. New evidence of the effect of the chemical structure of activated carbon on the activity to promote radical generation in an advanced oxidation process using hydrogen peroxide. *Micropor. Mesopor. Mat.* **2018**, *259*, 1–8. [CrossRef]

61. Martin-Martinez, M.; Álvarez-Torrellas, S.; García, J.; Silva, A.M.T.; Faria, J.L.; Gomes, H.T. Exploring the activity of chemical-activated carbons synthesized from peach stones as metal-free catalysts for wet peroxide oxidation. *Catal. Today* **2018**, *313*, 20–25. [CrossRef]

62. Martin-Martinez, M.; Machado, B.F.; Serp, P.; Morales-Torres, S.; Silva, A.M.T.; Figueiredo, J.L.; Faria, J.L.; Gomes, H.T. Carbon nanotubes as catalysts for wet peroxide oxidation: The effect of surface chemistry. *Catal. Today* **2020**, *357*, 332–340. [CrossRef]

63. Ribeiro, R.S.; Silva, A.M.T.; Figueiredo, J.L.; Faria, J.L.; Gomes, H.T. Catalytic wet peroxide oxidation: A route towards the application of hybrid magnetic carbon nanocomposites for the degradation of organic pollutants. A review. *Appl. Catal. B.* **2016**, *187*, 428–460. [CrossRef]

64. Duan, X.; Sun, H.; Wang, S. Metal-Free Carbocatalysis in Advanced Oxidation Reactions. *Acc. Chem. Res.* **2018**, *51*, 678–687. [CrossRef]

65. Xiao, P.-f.; An, L.; Wu, D.-d. The use of carbon materials in persulfate-based advanced oxidation processes: A review. *New Carbon Mater.* **2020**, *35*, 667–683. [CrossRef]

66. He, X.; Zheng, N.; Hu, R.; Hu, Z.; Yu, J.C. Hydrothermal and Pyrolytic Conversion of Biomasses into Catalysts for Advanced Oxidation Treatments. *Adv. Funct. Mater.* **2020**, *31*, 2006505. [CrossRef]

67. Rocha, R.P.; Pereira, M.F.R.; Figueiredo, J.L. Metal-free carbon materials as catalysts for wet air oxidation. *Catal. Today* **2020**, *356*, 189–196. [CrossRef]

68. Vieira, O.; Ribeiro, R.S.; Diaz de Tuesta, J.L.; Gomes, H.T.; Silva, A.M.T. A systematic literature review on the conversion of plastic wastes into valuable 2D graphene-based materials. *Chem. Eng. J.* **2021**, *428*, 131399. [CrossRef]

69. González-García, P. Activated carbon from lignocellulosics precursors: A review of the synthesis methods, characterization techniques and applications. *Renew. Sustain. Energy Rev.* **2018**, *82*, 1393–1414. [CrossRef]

70. Vivekanandhan, S.; Schreiber, M.; Muthuramkumar, S.; Misra, M.; Mohanty, A.K. Carbon nanotubes from renewable feedstocks: A move toward sustainable nanofabrication. *J. Appl. Polym. Sci.* **2017**, *134*, 44255. [CrossRef]

71. Kumar, M.; Ando, Y. Chemical vapor deposition of carbon nanotubes: A review on growth mechanism and mass production. *J. Nanosci. Nanotechnol.* **2020**, *10*, 3739–3758. [CrossRef]

72. Das, R.; Shahnavaz, Z.; Ali, M.E.; Islam, M.M.; Abd Hamid, S.B. Can We Optimize Arc Discharge and Laser Ablation for Well-Controlled Carbon Nanotube Synthesis? *Nanoscale Res. Lett.* **2016**, *11*, 510. [CrossRef] [PubMed]

73. Edwards, R.S.; Coleman, K.S. Graphene synthesis: Relationship to applications. *Nanoscale* **2013**, *5*, 38–51. [CrossRef] [PubMed]

74. Kong, L.; Wang, J.; Ma, F.; Sun, M.; Quan, J. Graphitic carbon nitride nanostructures: Catalysis. *Appl. Mater. Today* **2019**, *16*, 388–424. [CrossRef]

75. Rono, N.; Kibet, J.K.; Martincigh, B.S.; Nyamori, V.O. A review of the current status of graphitic carbon nitride. *Crit. Rev. Solid State Mater. Sci.* **2020**, *46*, 189–217. [CrossRef]

76. Rafiee, E.; Khodayari, M. Synthesis and characterization of PMoV/Fe$_3$O$_4$/g-C$_3$N$_4$ from melamine: An industrial green nanocatalyst for deep oxidative desulfurization. *Chin. J. Catal.* **2017**, *38*, 458–468. [CrossRef]

77. Meman, N.M.; Zarenezhad, B.; Rashidi, A.; Hajjar, Z.; Esmaeili, E. Application of palladium supported on functionalized MWNTs for oxidative desulfurization of naphtha. *J. Ind. Eng. Chem.* **2015**, *22*, 179–184. [CrossRef]

78. Zhu, Y.; Zhu, M.; Kang, L.; Yu, F.; Dai, B. Phosphotungstic Acid Supported on Mesoporous Graphitic Carbon Nitride as Catalyst for Oxidative Desulfurization of Fuel. *Ind. Eng. Chem. Res.* **2015**, *54*, 2040–2047. [CrossRef]

79. Meman, N.M.; Pourkhalil, M.; Rashidi, A.; ZareNezhad, B. Synthesis, characterization and operation of a functionalized multi-walled CNT supported MnOx nanocatalyst for deep oxidative desulfurization of sour petroleum fractions. *J. Ind. Eng. Chem.* **2014**, *20*, 4054–4058. [CrossRef]

80. Ugal, J.R.; Jima'a, R.B.; Al-Jubori, W.M.K.; Abbas, B.F.; Al-Jubori, N.M. Oxidative Desulfurization of Hydrotreated Gas Oil using Fe$_2$O$_3$ and Pd Loaded over Activated Carbon as Catalysts. *Orient. J. Chem.* **2018**, *34*, 1091–1097. [CrossRef]

81. Alwan, H.H.; Ali, A.A.; Makki, H.F. Optimization of Oxidative Desulfurization Reaction with Fe$_2$O$_3$ Catalyst Supported on Graphene Using Box-Behnken Experimental Method. *Bull. Chem. React. Eng. Catal.* **2020**, *15*, 175–185. [CrossRef]

82. Rafiee, E.; Joshaghani, M.; Ghaderi-Shekhi Abadi, P. Oxidative desulfurization of diesel by potato based-carbon as green support for H$_5$PMo$_{10}$V$_2$O$_{40}$: Efficient composite nanorod catalyst. *J. Saudi Chem. Soc.* **2017**, *21*, 599–609. [CrossRef]

83. Huang, P.; Liu, A.; Kang, L.; Dai, B.; Zhu, M.; Zhang, J. Heteropolyacid Supported on Nitrogen-doped Onion-Like Carbon as Catalyst for Oxidative Desulfurization. *ChemistrySelect* **2017**, *2*, 4010–4015. [CrossRef]

84. Rafiee, E.; Shahbazirad, A.; Khodayari, M. Preparation and characterization of nanocomposite of graphitic carbon nitride and TiO$_2$ as a porous support for nano catalyst for desulfurization process. *J. Saudi Chem. Soc.* **2017**, *21*, 943–953. [CrossRef]

85. Abdelrahman, A.A.; Betiha, M.A.; Rabie, A.M.; Ahmed, H.S.; Elshahat, M.F. Removal of refractory Organo-sulfur compounds using an efficient and recyclable {Mo$_{132}$} nanoball supported graphene oxide. *J. Mol. Liq.* **2018**, *252*, 121–132. [CrossRef]

86. Wang, C.; Li, A.; Xu, J.; Wen, J.; Zhang, H.; Zhang, L. Preparation of WO$_3$/CNT catalysts in presence of ionic liquid [C$_{16}$mim]Cl and catalytic efficiency in oxidative desulfurization. *J. Chem. Technol. Biotechnol.* **2019**, *94*, 3403–3412. [CrossRef]

87. Gao, Y.; Cheng, L.; Gao, R.; Hu, G.; Zhao, J. Deep desulfurization of fuels using supported ionic liquid-polyoxometalate hybrid as catalyst: A comparison of different types of ionic liquids. *J. Hazard. Mater.* **2021**, *401*, 123267. [CrossRef] [PubMed]

88. Zhuang, L.; Li, Q.; Chen, S.; Hou, X.; Lin, J. In-situ preparation of porous carbon-supported molybdenum dioxide and its performance in the oxidative desulfurization of thiophene. *J. Mater. Sci.* **2014**, *49*, 5606–5616. [CrossRef]

89. Gao, Y.; Liu, Z.; Gao, R.; Hu, G.; Zhao, J. Support ionic liquid-heteropolyacid hybrid on mesoporous carbon aerogel with a high surface area for highly efficient desulfurization under mild conditions. *Micropor. Mesopor. Mat.* **2020**, *305*, 110392. [CrossRef]

90. Rongxiang, Z.; Xiuping, L.; Jianxun, S.; Weiwei, S.; Xiaohan, G. The preparation of WO$_3$/C composite and its application in oxidative desulfurization of fuel. *China Pet. Process. Petrochem. Technol.* **2017**, *19*, 65–73.

91. Xiao, J.; Wu, L.; Wu, Y.; Liu, B.; Dai, L.; Li, Z.; Xia, Q.; Xi, H. Effect of gasoline composition on oxidative desulfurization using a phosphotungstic acid/activated carbon catalyst with hydrogen peroxide. *Appl. Energy* **2014**, *113*, 78–85. [CrossRef]

92. Bhadra, B.N.; Song, J.Y.; Khan, N.A.; Jhung, S.H. TiO$_2$-Containing Carbon Derived from a Metal–Organic Framework Composite: A Highly Active Catalyst for Oxidative Desulfurization. *ACS Appl. Mat. Interfaces* **2017**, *9*, 31192–31202. [CrossRef]

93. Khan, N.A.; Bhadra, B.N.; Park, S.W.; Han, Y.S.; Jhung, S.H. Tungsten Nitride, Well-Dispersed on Porous Carbon: Remarkable Catalyst, Produced without Addition of Ammonia, for the Oxidative Desulfurization of Liquid Fuel. *Small* **2020**, *16*, e1901564. [CrossRef]

94. Do Prado, N.T.; Heitmann, A.P.; Mansur, H.S.; Mansur, A.A.; Oliveira, L.C.A.; de Castro, C.S. PET-modified red mud as catalysts for oxidative desulfurization reactions. *J. Environ. Sci.* **2017**, *57*, 312–320. [CrossRef] [PubMed]

95. Wang, C.; Miao, Q.; Huang, X.; Li, J.; Duan, Y.; Yan, L.; Jiang, Y.; Lu, S. Fabrication of various morphological forms of a g-C$_3$N$_4$-supported MoO$_3$ catalyst for the oxidative desulfurization of dibenzothiophene. *New J. Chem.* **2020**, *44*, 18745–18755. [CrossRef]

96. Zhao, R.; Li, X.; Su, J.; Gao, X. Preparation of WO$_3$/g-C$_3$N$_4$ composites and their application in oxidative desulfurization. *Appl. Surf. Sci.* **2017**, *392*, 810–816. [CrossRef]

97. Zhu, J.; Wu, P.; Chen, L.; He, J.; Wu, Y.; Wang, C.; Chao, Y.; Lu, L.; He, M.; Zhu, W.; et al. 3D-printing of integrated spheres as a superior support of phosphotungstic acid for deep oxidative desulfurization of fuel. *J. Energy Chem.* **2020**, *45*, 91–97. [CrossRef]

98. Hou, L.-p.; Zhao, R.-x.; Li, X.-p.; Gao, X.-h. Preparation of MoO$_2$/g-C$_3$N$_4$ composites with a high surface area and its application in deep desulfurization from model oil. *Appl. Surf. Sci.* **2018**, *434*, 1200–1209. [CrossRef]

99. Ye, J.; Wen, J.; Zhao, D.; Zhang, P.; Li, A.; Zhang, L.; Zhang, H.; Wu, M. Macroporous 3D carbon-nitrogen (CN) confined MoO$_x$ catalyst for enhanced oxidative desulfurization of dibenzothiophene. *Chin. Chem. Lett.* **2020**, *31*, 2819–2824. [CrossRef]

100. Ghubayra, R.; Nuttall, C.; Hodgkiss, S.; Craven, M.; Kozhevnikova, E.F.; Kozhevnikov, I.V. Oxidative desulfurization of model diesel fuel catalyzed by carbon-supported heteropoly acids. *Appl. Catal. B* **2019**, *253*, 309–316. [CrossRef]

101. Wang, R.; Yu, F.; Zhang, G.; Zhao, H. Performance evaluation of the carbon nanotubes supported Cs$_{2.5}$H$_{0.5}$PW$_{12}$O$_{40}$ as efficient and recoverable catalyst for the oxidative removal of dibenzothiophene. *Catal. Today* **2010**, *150*, 37–41. [CrossRef]

102. Xing, P.; Zhao, R.; Li, X.; Gao, X. Preparation of CoWO$_4$/g-C$_3$N$_4$ and its Ultra-Deep Desulfurization Property. *Aust. J. Chem.* **2017**, *70*, 271. [CrossRef]

103. Quyen, N.D.V.; Tuyen, T.N.; Khieu, D.Q.; Hai, H.V.M.; Tin, D.X.; Itatani, K. Oxidation of dibenzothiophene using the heterogeneous catalyst of tungsten-based carbon nanotubes. *Green Process. Synth.* **2019**, *8*, 68–77. [CrossRef]

104. Wang, Q.; Wang, S.; Yu, H. Oxidative desulphurization of model fuel by in situ produced hydrogen peroxide on palladium/active carbon. *Can. J. Chem. Eng.* **2017**, *95*, 136–141. [CrossRef]

105. Yu, G.X.; Zhou, R.X.; Li, J.B.; Zhou, X.L.; Li, C.L.; Chen, L.F.; Wang, J.A. Oxidative Removal of Dibenzothiophene by H$_2$O$_2$ over Activated Carbon-Supported Phosphotungstic Acid Catalysts. *Adv. Mat. Res.* **2010**, *132*, 126–132. [CrossRef]

106. Kermani, A.M.; Ahmadpour, A.; Bastami, T.R.; Ghahramaninezhad, M. Deep oxidative desulfurization of dibenzothiophene with {Mo-132} nanoballs supported on activated carbon as an efficient catalyst at room temperature. *New J. Chem.* **2018**, *42*, 12188–12197. [CrossRef]

107. Liu, L.; Zhang, Y.; Tan, W. Ultrasound-assisted oxidation of dibenzothiophene with phosphotungstic acid supported on activated carbon. *Ultrason. Sonochem.* **2014**, *21*, 970–974. [CrossRef]

108. Liu, L.; Zhang, Y.; Tan, W. Synthesis and characterization of phosphotungstic acid/activated carbon as a novel ultrasound oxidative desulfurization catalyst. *Front. Chem. Sci. Eng.* **2013**, *7*, 422–427. [CrossRef]

109. Piccinino, D.; Abdalghani, I.; Botta, G.; Crucianelli, M.; Passacantando, M.; Di Vacri, M.L.; Saladino, R. Preparation of wrapped carbon nanotubes poly(4-vinylpyridine)/MTO based heterogeneous catalysts for the oxidative desulfurization (ODS) of model and synthetic diesel fuel. *Appl. Catal. B* **2017**, *200*, 392–401. [CrossRef]

110. Dini, Z.; Afsharpour, M.; Tabar-Heydar, K. UV-assisted functionalization of carbon nanotube for synthesis of efficient desulfurization catalysts (NH$_2$/COOH)-MWNT/MoO$_3$. *Diam. Relat. Mat.* **2019**, *91*, 237–246. [CrossRef]

111. Afsharpour, M.; Dini, Z. One-pot functionalization of carbon nanotubes by WO_3/MoO_3 nanoparticles as oxidative desulfurization catalysts. *Fuller. Nanotub. Carbon Nanostructures* **2018**, *27*, 198–205. [CrossRef]

112. Bhadra, B.N.; Khan, N.A.; Jhung, S.H. Co supported on N-doped carbon, derived from bimetallic azolate framework-6: A highly effective oxidative desulfurization catalyst. *J. Mat. Chem. A* **2019**, *7*, 17823–17833. [CrossRef]

113. Liao, X.; Huang, Y.; Zhou, Y.; Liu, H.; Cai, Y.; Lu, S.; Yao, Y. Homogeneously dispersed HPW/graphene for high efficient catalytic oxidative desulfurization prepared by electrochemical deposition. *Appl. Surf. Sci.* **2019**, *484*, 917–924. [CrossRef]

114. Ma, R.; Guo, J.; Wang, D.; He, M.; Xun, S.; Gu, J.; Zhu, W.; Li, H. Preparation of highly dispersed WO_3/few layer g-C_3N_4 and its enhancement of catalytic oxidative desulfurization activity. *Colloids Surf. A Physicochem. Eng. Asp.* **2019**, *572*, 250–258. [CrossRef]

115. Chen, K.; Zhang, X.-M.; Yang, X.-F.; Jiao, M.-G.; Zhou, Z.; Zhang, M.-H.; Wang, D.-H.; Bu, X.-H. Electronic structure of heterojunction MoO_2/g-C_3N_4 catalyst for oxidative desulfurization. *Appl. Catal. B* **2018**, *238*, 263–273. [CrossRef]

116. Xun, S.; Ti, Q.; Wu, L.; He, M.; Wang, C.; Chen, L.; Yang, W.; Zhu, L.; Zhu, W.; Li, H. Few Layer g-C_3N_4 Dispersed Quaternary Phosphonium Ionic Liquid for Highly Efficient Catalytic Oxidative Desulfurization of Fuel. *Energy Fuels* **2020**, *34*, 12379–12387. [CrossRef]

117. Gu, J.; Liu, M.; Xun, S.; He, M.; Wu, L.; Zhu, L.; Wu, X.; Zhu, W.; Li, H. Lipophilic decavanadate supported by three-dimensional porous carbon nitride catalyst for aerobic oxidative desulfurization. *Mol. Catal.* **2020**, *483*, 110709. [CrossRef]

118. Chen, S.; Lu, W.; Yao, Y.; Chen, H.; Chen, W. Oxidative desulfurization of dibenzothiophene with molecular oxygen catalyzed by carbon fiber-supported iron phthalocyanine. *React. Kinet. Mech. Catal.* **2013**, *111*, 535–547. [CrossRef]

119. Xun, S.; Ti, Q.; Jiao, Z.; Wu, L.; He, M.; Chen, L.; Zhu, L.; Zhu, W.; Li, H. Dispersing TiO_2 Nanoparticles on Graphite Carbon for an Enhanced Catalytic Oxidative Desulfurization Performance. *Ind. Eng. Chem. Res.* **2020**, *59*, 18471–18479. [CrossRef]

120. Gao, Y.; Lv, Z.; Gao, R.; Hu, G.; Zhao, J. Dawson type polyoxometalate based-poly ionic liquid supported on different carbon materials for high-efficiency oxidative desulfurization with molecular oxygen as the oxidant. *New J. Chem.* **2020**, *44*, 20358–20366. [CrossRef]

121. Chen, L.; Ren, J.-T.; Yuan, Z.-Y. Atomic heterojunction-induced electron interaction in P-doped g-C_3N_4 nanosheets supported V-based nanocomposites for enhanced oxidative desulfurization. *Chem. Eng. J.* **2020**, *387*, 124164. [CrossRef]

122. Zou, J.; Lin, Y.; Wu, S.; Zhong, Y.; Yang, C. Molybdenum Dioxide Nanoparticles Anchored on Nitrogen-Doped Carbon Nanotubes as Oxidative Desulfurization Catalysts: Role of Electron Transfer in Activity and Reusability. *Adv. Funct. Mat.* **2021**, *31*, 2100442. [CrossRef]

123. Wang, C.; Zhu, W.; Xu, Y.; Xu, H.; Zhang, M.; Chao, Y.; Yin, S.; Li, H.; Wang, J. Preparation of TiO_2/g-C_3N_4 composites and their application in photocatalytic oxidative desulfurization. *Ceram. Int.* **2014**, *40*, 11627–11635. [CrossRef]

124. Li, X.; Zhu, W.; Lu, X.; Zuo, S.; Yao, C.; Ni, C. Integrated nanostructures of CeO_2/attapulgite/g-C_3N_4 as efficient catalyst for photocatalytic desulfurization: Mechanism, kinetics and influencing factors. *Chem. Eng. J.* **2017**, *326*, 87–98. [CrossRef]

125. Ma, S.; Li, X.; Lu, X.; Zuo, S.; Li, Z.; Yao, C. Carbon quantum dots/attapulgite nanocomposites with enhanced photocatalytic performance for desulfurization. *J. Mater. Sci.: Mater. Electron.* **2017**, *29*, 2709–2715. [CrossRef]

126. Zhang, G.; Ren, J.; Zhao, W.; Tian, M.; Chen, W. Photocatalytic desulfurization of thiophene base on molecular oxygen and zinc phthalocyanine/g-C_3N_4. *Res. Chem. Intermed.* **2018**, *44*, 5547–5557. [CrossRef]

127. Vu, T.H.T.; Nguyen, T.T.T.; Nguyen, P.H.T.; Do, M.H.; Au, H.T.; Nguyen, T.B.; Nguyen, D.L.; Park, J.S. Fabrication of photocatalytic composite of multi-walled carbon nanotubes/TiO_2 and its application for desulfurization of diesel. *Mater. Res. Bull.* **2012**, *47*, 308–314. [CrossRef]

128. Jiang, W.; Zheng, D.; Xun, S.; Qin, Y.; Lu, Q.; Zhu, W.; Li, H. Polyoxometalate-based ionic liquid supported on graphite carbon induced solvent-free ultra-deep oxidative desulfurization of model fuels. *Fuel* **2017**, *190*, 1–9. [CrossRef]

129. Astle, M.A.; Rance, G.A.; Loughlin, H.J.; Peters, T.D.; Khlobystov, A.N. Molybdenum Dioxide in Carbon Nanoreactors as a Catalytic Nanosponge for the Efficient Desulfurization of Liquid Fuels. *Adv. Funct. Mat.* **2019**, *29*, 1808092. [CrossRef]

130. Kampouraki, Z.C.; Giannakoudakis, D.A.; Triantafyllidis, K.S.; Deliyanni, E.A. Catalytic oxidative desulfurization of a 4,6-DMDBT containing model fuel by metal-free activated carbons: The key role of surface chemistry. *Green Chem.* **2019**, *21*, 6685–6698. [CrossRef]

131. He, J.; Wu, P.; Lu, L.; Sun, H.; Jia, Q.; Hua, M.; He, M.; Xu, C.; Zhu, W.; Li, H. Synthesis of N,O-Doped Porous Graphene from Petroleum Coke for Deep Oxidative Desulfurization of Fuel. *Energy Fuels* **2019**, *33*, 8302–8311. [CrossRef]

132. Gonzalez, L.A.; Kracke, P.; Green, W.H.; Tester, J.W.; Shafer, L.M.; Timko, M.T. Oxidative Desulfurization of Middle-Distillate Fuels Using Activated Carbon and Power Ultrasound. *Energy Fuels* **2012**, *26*, 5164–5176. [CrossRef]

133. Haw, K.-G.; Bakar, W.A.W.A.; Ali, R.; Chong, J.-F.; Kadir, A.A.A. Catalytic oxidative desulfurization of diesel utilizing hydrogen peroxide and functionalized-activated carbon in a biphasic diesel–acetonitrile system. *Fuel Process. Technol.* **2010**, *91*, 1105–1112. [CrossRef]

134. Gu, Q.; Ding, Y.; Liu, Z.; Lin, Y.; Schlögl, R.; Heumann, S.; Su, D. Probing the intrinsic catalytic activity of carbon nanotubes for the metal-free oxidation of aromatic thiophene compounds in ionic liquids. *J. Energy Chem.* **2019**, *32*, 131–137. [CrossRef]

135. Gu, Q.; Wen, G.; Ding, Y.; Wu, K.-H.; Chen, C.; Su, D. Reduced graphene oxide: A metal-free catalyst for aerobic oxidative desulfurization. *Green Chem.* **2017**, *19*, 1175–1181. [CrossRef]

136. Zhang, W.; Zhang, H.; Xiao, J.; Zhao, Z.; Yu, M.; Li, Z. Carbon nanotube catalysts for oxidative desulfurization of a model diesel fuel using molecular oxygen. *Green Chem.* **2014**, *16*, 211–220. [CrossRef]

137. Zeng, X.; Xiao, X.; Li, Y.; Chen, J.; Wang, H. Deep desulfurization of liquid fuels with molecular oxygen through graphene photocatalytic oxidation. *Appl. Catal. B* **2017**, *209*, 98–109. [CrossRef]

138. Timko, M.T.; Wang, J.A.; Burgess, J.; Kracke, P.; Gonzalez, L.; Jaye, C.; Fischer, D.A. Roles of surface chemistry and structural defects of activated carbons in the oxidative desulfurization of benzothiophenes. *Fuel* **2016**, *163*, 223–231. [CrossRef]

139. Abdi, G.; Ashokkumar, M.; Alizadeh, A. Ultrasound-assisted oxidative-adsorptive desulfurization using highly acidic graphene oxide as a catalyst-adsorbent. *Fuel* **2017**, *210*, 639–645. [CrossRef]

140. Liu, H.; Li, Z.; Dong, J.; Liu, D.; Liu, C.; Chi, Y.; Hu, C. Polyoxometalates encapsulated into hollow double-shelled nanospheres as amphiphilic nanoreactors for an effective oxidative desulfurization. *Nanoscale* **2020**, *12*, 16586–16595. [CrossRef]

141. Yu, Z.; Huang, X.; Xun, S.; He, M.; Zhu, L.; Wu, L.; Yuan, M.; Zhu, W.; Li, H. Synthesis of carbon nitride supported amphiphilic phosphotungstic acid based ionic liquid for deep oxidative desulfurization of fuels. *J. Mol. Liq.* **2020**, *308*, 113059. [CrossRef]

142. Li, X.; Yang, X.; Zhou, F.; Zhang, J.; Yang, H.; Wang, Y.; Zhao, Y.; Yuan, X.; Ju, J.; Hu, S. Construction of novel amphiphilic [Bmin]₃PMo₁₂O₄₀/g-C₃N₄ heterojunction catalyst with outstanding photocatalytic oxidative desulfurization performance under visible light. *J. Taiwan Inst. Chem. Eng.* **2019**, *100*, 210–219. [CrossRef]

143. Mambrini, R.V.; Maia, C.Z.; Ardisson, J.D.; de Souza, P.P.; Moura, F.C.C. Fe/C and FeMo/C hybrid materials for the biphasic oxidation of fuel contaminants. *New J. Chem.* **2017**, *41*, 142–150. [CrossRef]

144. Oliveira, A.A.S.; Christofani, T.; Teixeira, I.F.; Ardisson, J.D.; Moura, F.C.C. Magnetic amphiphilic nanocomposites based on silica–carbon for sulphur contaminant oxidation. *New J. Chem.* **2015**, *39*, 5445–5452. [CrossRef]

145. Oliveira, A.A.S.; Teixeira, I.F.; Christofani, T.; Tristão, J.C.; Guimarães, I.R.; Moura, F.C.C. Biphasic oxidation reactions promoted by amphiphilic catalysts based on red mud residue. *Appl. Catal. B* **2014**, *144*, 144–151. [CrossRef]

146. Teixeira, I.F.; da Silva Oliveira, A.A.; Christofani, T.; Moura, F.C.C. Biphasic oxidation promoted by magnetic amphiphilic nanocomposites undergoing a reversible emulsion process. *J. Mat. Chem. A* **2013**, *1*, 10203–10208. [CrossRef]

147. Dou, S.-Y.; Wang, R. The C-Si Janus nanoparticles with supported phosphotungstic active component for Pickering emulsion desulfurization of fuel oil without stirring. *Chem. Eng. J.* **2019**, *369*, 64–76. [CrossRef]

148. Hasannia, S.; Kazemeini, M.; Rashidi, A.; Seif, A. The oxidative desulfurization process performed upon a model fuel utilizing modified molybdenum based nanocatalysts: Experimental and density functional theory investigations under optimally prepared and operated conditions. *Appl. Surf. Sci.* **2020**, *527*, 146798. [CrossRef]

149. Abdullah, W.N.W.; Bakar, W.A.W.A.; Abdullah, N.H.; Mokhtar, W.N.A.W.; Rosid, S.J.M.; Shukri, N.M. Effect of activated carbon supported Ce/Fe based catalyst for catalytic oxidative desulfurization of Malaysian diesel fuel. *AIP Conf. Proc.* **2019**, *2068*, 020075. [CrossRef]

150. Dizaji, A.K.; Mokhtarani, B.; Mortaheb, H.R. Deep and fast oxidative desulfurization of fuels using graphene oxide-based phosphotungstic acid catalysts. *Fuel* **2019**, *236*, 717–729. [CrossRef]

151. Dizaji, A.K.; Mortaheb, H.R.; Mokhtarani, B. Complete oxidative desulfurization using graphene oxide-based phosphomolybdic acid catalyst: Process optimization by two phase mass balance approach. *Chem. Eng. J.* **2018**, *335*, 362–372. [CrossRef]

152. Tamborrino, V.; Costamagna, G.; Bartoli, M.; Rovere, M.; Jagdale, P.; Lavagna, L.; Ginepro, M.; Tagliaferro, A. Catalytic oxidative desulphurization of pyrolytic oils to fuels over different waste derived carbon-based catalysts. *Fuel* **2021**, *296*, 120693. [CrossRef]

153. Gao, Y.; Gao, R.; Zhang, G.; Zheng, Y.; Zhao, J. Oxidative desulfurization of model fuel in the presence of molecular oxygen over polyoxometalate based catalysts supported on carbon nanotubes. *Fuel* **2018**, *224*, 261–270. [CrossRef]

154. Gao, Y.; Lv, Z.; Gao, R.; Zhang, G.; Zheng, Y.; Zhao, J. Oxidative desulfurization process of model fuel under molecular oxygen by polyoxometalate loaded in hybrid material CNTs@MOF-199 as catalyst. *J. Hazard. Mat.* **2018**, *359*, 258–265. [CrossRef] [PubMed]

155. Jiang, W.; Xiao, J.; Dong, L.; Wang, C.; Li, H.; Luo, Y.; Zhu, W.; Li, H. Polyoxometalate-Based Poly(ionic liquid) as a Precursor for Superhydrophobic Magnetic Carbon Composite Catalysts toward Aerobic Oxidative Desulfurization. *ACS Sustain. Chem. Eng.* **2019**, *7*, 15755–15761. [CrossRef]

156. Wang, Y.; Zhang, G.; Guan, T.; Xu, F.; Wu, J.; Zhou, E.; Wang, J.; Li, K. Ultra-Deep Oxidative Desulfurization of Model Oil Catalyzed by In Situ Carbon-Supported Vanadium Oxides Using Cumene Hydroperoxide as Oxidant. *ChemistrySelect* **2020**, *5*, 2148–2156. [CrossRef]

157. Timko, M.T.; Schmois, E.; Patwardhan, P.; Kida, Y.; Class, C.A.; Green, W.H.; Nelson, R.K.; Reddy, C.M. Response of Different Types of Sulfur Compounds to Oxidative Desulfurization of Jet Fuel. *Energy Fuels* **2014**, *28*, 2977–2983. [CrossRef]

158. Zhang, Y.; Wang, R. Synthesis of silica@C-dots/phosphotungstates core-shell microsphere for effective oxidative-adsorptive desulfurization of dibenzothiophene with less oxidant. *Appl. Catal. B* **2018**, *234*, 247–259. [CrossRef]

159. Guimarães, I.R.; Giroto, A.S.; de Souza, W.F.; Guerreiro, M.C. Highly reactive magnetite covered with islands of carbon: Oxidation of N and S-containing compounds in a biphasic system. *Appl. Catal. A* **2013**, *450*, 106–113. [CrossRef]

160. Oliveira, A.A.S.; Costa, D.A.S.; Teixeira, I.F.; Moura, F.C.C. Gold nanoparticles supported on modified red mud for biphasic oxidation of sulfur compounds: A synergistic effect. *Appl. Catal. B* **2015**, *162*, 475–482. [CrossRef]

161. Rezvani, M.A.; Shaterian, M.; Shokri Aghbolagh, Z.; Babaei, R. Oxidative desulfurization of gasoline catalyzed by IMID@PMA@CS nanocomposite as a high-performance amphiphilic nanocatalyst. *Environ. Progress Sustain. Energy* **2018**, *37*, 1891–1900. [CrossRef]

162. Diaz de Tuesta, J.L.; Saviotti, M.C.; Roman, F.F.; Pantuzza, G.F.; Sartori, H.J.F.; Shinibekova, A.; Kalmakhanova, M.S.; Massalimova, B.K.; Pietrobelli, J.M.T.A.; Lenzi, G.G.; et al. Assisted hydrothermal carbonization of agroindustrial byproducts as effective step in the production of activated carbon catalysts for wet peroxide oxidation of micro-pollutants. *J. Environ. Chem. Eng.* **2021**, *9*, 105004. [CrossRef]

163. Santos Silva, A.; Seitovna Kalmakhanova, M.; Kabykenovna Massalimova, B.; Sgorlon, J.G.; Diaz de Tuesta, J.L.; Gomes, H.T. Wet Peroxide Oxidation of Paracetamol Using Acid Activated and Fe/Co-Pillared Clay Catalysts Prepared from Natural Clays. *Catalysts* **2019**, *9*, 705. [CrossRef]

164. Souza, W.F.; Pereira, M.C.; Oliveira, L.C.A. Amphiphilic catalysts based on onion-like carbon over magnetic iron oxide for petrochemical industry use. *Fuel* **2012**, *96*, 604–607. [CrossRef]

165. Oliveira, A.A.S.; Martins, A.R.; Ferreira, R.V.; Cunha, I.T.; Serp, P.; de Mesquita, J.P.; Moura, F.C.C. N-doped carbon nanotubes grown on red mud residue: Hybrid nanocomposites for technological applications. *Catal. Today* **2020**, *344*, 247–258. [CrossRef]

166. Purceno, A.D.; Machado, B.F.; Teixeira, A.P.; Medeiros, T.V.; Benyounes, A.; Beausoleil, J.; Menezes, H.C.; Cardeal, Z.L.; Lago, R.M.; Serp, P. Magnetic amphiphilic hybrid carbon nanotubes containing N-doped and undoped sections: Powerful tensioactive nanostructures. *Nanoscale* **2015**, *7*, 294–300. [CrossRef] [PubMed]

167. Ammar, S.H.; Kareem, Y.S.; Mohammed, M.S. Catalytic-oxidative/adsorptive denitrogenation of model hydrocarbon fuels under ultrasonic field using magnetic reduced graphene oxide-based phosphomolybdic acid (PMo-Fe_3O_4/rGO). *Ultrason. Sonochem.* **2020**, *64*, 105050. [CrossRef] [PubMed]

168. Bhadra, B.N.; Song, J.Y.; Uddin, N.; Khan, N.A.; Kim, S.; Choi, C.H.; Jhung, S.H. Oxidative denitrogenation with TiO_2@porous carbon catalyst for purification of fuel: Chemical aspects. *Appl. Catal. B* **2019**, *240*, 215–224. [CrossRef]

169. Diniz, C.V.; Nascimento, J.V.; Binatti, I.; Freitas, P.E.; Mambrini, R.V. Hybrid catalysts based on waste electrical and electronic equipment supported on bentonite for the removal of contaminants compounds in liquid phase. *Catal. Today* **2020**, *344*, 75–83. [CrossRef]

170. Martin-Martinez, M.; Ribeiro, R.S.; Machado, B.F.; Serp, P.; Morales-Torres, S.; Silva, A.M.T.; Figueiredo, J.L.; Faria, J.L.; Gomes, H.T. Role of Nitrogen Doping on the Performance of Carbon Nanotube Catalysts: A Catalytic Wet Peroxide Oxidation Application. *ChemCatChem* **2016**, *8*, 2068–2078. [CrossRef]

171. Diaz de Tuesta, J.L.; Quintanilla, A.; Casas, J.A.; Morales-Torres, S.; Faria, J.L.; Silva, A.M.T.; Gomes, H.T. The pH effect on the kinetics of 4-nitrophenol removal by CWPO with doped carbon black catalysts. *Catal. Today* **2020**, *356*, 216–225. [CrossRef]

172. Diaz de Tuesta, J.L.; Machado, B.F.; Serp, P.; Silva, A.M.T.; Faria, J.L.; Gomes, H.T. Janus amphiphilic carbon nanotubes as Pickering interfacial catalysts for the treatment of oily wastewater by selective oxidation with hydrogen peroxide. *Catal. Today* **2020**, *356*, 205–215. [CrossRef]